AD-A053 785   NAVAL RESEARCH LAB   WASHINGTON D C   F/G 18/1
                NUMERICAL STUDIES OF COMPRESSIBILITY EFFECTS IN ROTATING IMPLOD--ETC(U)
                JAN 78 D L BOOK, P J TURCHI   E(49-20)-1006
UNCLASSIFIED   NRL-MR-3699   SBIE-AD-E000 138   NL

| OF |
AD
A053 785

END
DATE
FILMED
6-78
DDC

3/28/78

ade 000138

AD A053785

AD No.
DDC FILE COPY

Numerical Studies of Compressibility Effects in Rotating Imploding Liquid Liners

D. L. Book and P. J. Turchi

Plasma Physics Division

(14)
B.S.

January 1978

D D C
RECEIVED
MAY 11 1978
B

NAVAL RESEARCH LABORATORY
Washington, D.C.

REPORT DOCUMENTATION PAGE	READ INSTRUCTIONS BEFORE COMPLETING FORM

1. REPORT NUMBER NRL-MR— NRL Memorandum Report 3699	2. GOVT ACCESSION NO.	3. RECIPIENT'S CATALOG NUMBER

4. TITLE *(and Subtitle)* NUMERICAL STUDIES OF COMPRESSIBILITY EFFECTS IN ROTATING IMPLODING LIQUID LINERS.	5. TYPE OF REPORT & PERIOD COVERED Interim report on a continuing NRL problem
	6. PERFORMING ORG. REPORT NUMBER

7. AUTHOR(s) D. L. Book and P. J. Turchi	8. CONTRACT OR GRANT NUMBER(s)

9. PERFORMING ORGANIZATION NAME AND ADDRESS Naval Research Laboratory Washington, D.C. 20375	10. PROGRAM ELEMENT, PROJECT, TASK AREA & WORK UNIT NUMBERS NRL Problem H02-37 Project D.O.E. E(49-20)-1006

11. CONTROLLING OFFICE NAME AND ADDRESS	12. REPORT DATE January 1978
	13. NUMBER OF PAGES 54

14. MONITORING AGENCY NAME & ADDRESS*(if different from Controlling Office)* 55 p.	15. SECURITY CLASS. *(of this report)* UNCLASSIFIED
	15a. DECLASSIFICATION/DOWNGRADING SCHEDULE

16. DISTRIBUTION STATEMENT *(of this Report)*

Approved for public release; distribution unlimited.

17. DISTRIBUTION STATEMENT *(of the abstract entered in Block 20, if different from Report)*

SBIE   AD-E000 138

18. SUPPLEMENTARY NOTES

This research was sponsored by the U.S. Department of Energy.

19. KEY WORDS *(Continue on reverse side if necessary and identify by block number)*

Liners
Compressibility
Rayleigh-Taylor instability
Fusion

20. ABSTRACT *(Continue on reverse side if necessary and identify by block number)*

The final (minimum radius) state variables of a cylindrically imploded rotating liquid liner are computed as functions of p_f, the maximum compression achieved, and u_∞, the velocity the liner would attain if allowed to expand without restraint. For each choice of p_f and u_∞, the rotational speed is chosen to just stabilize the Rayleigh-Taylor modes on the inside surface. The acceleration of the inner surface is largest prior to turnaround, so that the rotational speed required for stabilization is close to that found for an equivalent incompressible liner. Near turnaround
(Continues)

DD $_{1\ JAN\ 73}^{FORM}$ 1473   EDITION OF 1 NOV 65 IS OBSOLETE
S/N 0102-014-6601

i

20. Abstract (Continued)

the inner portion of the liner becomes significantly compressed, making the efficiency with which the payload plasma is heated considerably less than that for an incompressible liner. The liner compression produced at turnaround alters the implosion dynamics and creates a pressure pulse propagating outward analogous to a "water hammer." An important favorable effect of compression is to extend the dwell period, during which thermonuclear reaction rates are maximal. The dependence of compression efficiency and of Q, defined as the ratio of thermonuclear yield to total system energy, on p_f and u_∞ are displayed for the parameter range of experimental interest. These results are then used to scale the system size in terms of allowable mechanical stress to indicate optimal peak operating pressures. The sidewall and endwall pressure loads are calculated for the same parameter range.

at infinity

sub f

ii

CONTENTS

iii

NUMERICAL STUDIES OF COMPRESSIBILITY EFFECTS IN ROTATING IMPLODING LIQUID LINERS

I.   Introduction

The Linus program at the Naval Research Laboratory is aimed at investigating the possibility of developing controlled thermonuclear fusion by adiabatically compressing plasma by <u>controlled</u> liner implosion.[1] The concept is based on the use of liquid metal liners (rather than the solid liners used in early experiments[2-5]) stabilized by rotation[6,7] and imploded hydraulically by high-pressure gas-driven pistons. Working with a liner which implodes cyclically, rather than disintegrating at each shot, permits recovery of much of the driving energy. This means that the system can operate at much lower values of Q, here defined as the ratio of the fusion yield to the total energy imparted to the liner. Since the volume and the total energy of a reactor system scale roughly as the square of Q, substantial reduction in reactor size becomes possible in principle.

The adoption of a "captive" (piston-driven) liquid liner design[1] eliminates the outer free surface, which if present would necessarily exhibit Rayleigh-Taylor instability near the outer turning point (i.e., at the onset of the implosion and near the end of the re-expansion phase). Thus, exploitation of the liquid properties is essential to the operation of a repetitively pulsed liner.

In this paper we examine closely a different aspect of liquid liners, namely, the effects of the finite compressibility found in real liquid metals. Measured by the simplest criterion, the flow Mach numbers M (relative to c, the speed of sound in the uncompressed material), these effects might be expected to be small or even negligible. In liquid alkali metals, for example, $c \approx 1.5\text{-}7.5$ km/sec, whereas the liner speeds attainable with hydraulic compression tend to be on the order of a few hundred meters per second, so that $M \sim .05\text{-}.2$. (These values are typical during most of the implosion; just prior to turnaround, speeds approaching 1 km/sec are achieved

1

due to convergence effects.) But even though the gross dynamics of an implosion is practically incompressible, the parameter of most concern to us - the amount of plasma compression - is greatly affected. For thermonuclear applications the liner has to be very thick relative to the inner radius at turnaround; volumetric compressions $\sim 10^3$, i.e., aspect ratios ~ 30, are typical. For a given value of the outer radius, an average compression throughout the liner of as little as 0.1% can double this inner radius and reduce the temperature achieved by a factor $\sim 2^{4/3} \approx 2.5$

Another deleterious effect of compressibility, known as "water hammer," arises from the nature of sound wave propagation in liquids. The liner is stopped so abruptly at turnaround by the buildup of pressure in the "payload" (the mixture of plasma and magnetic flux being compressed) that a compression wave is launched outward, followed by a rarefaction wave. This pressure pulse propagates to the side- and endwalls of the system, producing stresses equal to a significant fraction of the peak payload pressure and therefore substantially in excess of the initial driving pressure. Such loads can lead to failure of rigid structural members of the device.

While carrying out numerical studies of these phenomena, however, we discovered that the news is not all bad. During and immediately after turnaround the outer portion of a compressible liner continues to implode and compress the innermost portion. While this continues (roughly twice the sound transit time, defined as the liner thickness d divided by c) the liner inner radius expands at a slower speed than that with which it imploded. This prolongs the "dwell" of the liner, thereby enhancing Q. The effect is naturally more pronounced at high Mach numbers and with thicker liners.

There is considerable uncertainty about the appropriate form for the equation of state of liquid metals at high pressures and temperatures. Earlier treatments concentrated on the behavior of solid liners. Knoepfel[8] summarized the available measurements and theoretical models and quoted a quasi-empirical formula of Somon[9] for pressures less than 1 Mbar. We use this form below in our calculations even though it was derived for solid state. For

2

hydrodynamic applications the exact functional form turns out not to be important, since at Linus pressures ($p_{max} \sim 10^4 - 10^5$ bar) the velocity of sound deviates only slightly from its zero-pressure value.

The model studied in the present paper differs in significant respects from those treated in previous work. Earlier treatments all left rotation out of the picture; in Linus, by contrast, when Rayleigh-Taylor instability is fully suppressed, roughly half of the system energy ends up as rotational energy. In addition, previous treatments are inappropriate for Linus-type devices in other ways. For example, Lehner et al[10] studied magnetic flux compression produced by a slab liner, which relates closely to the cylindrical case only if the liner thickness d is much less than the final radius r_f. They introduced the concept of the effective thickness d^*, defined as the thickness an incompressible liner with the same density ρ would have to have to produce the same final payload pressure p_f for a given initial liner displacement $r_i \gg r_f$ and implosion speed $u_i = M_i c$. Only that portion of the liner within a distance d^* from the inner surface can participate effectively in the compression.

The results they obtained may be summarized as follows. The effective thickness is given by

$$\frac{d^*}{r_i} = 2 \left(\frac{p_i}{\rho c u_i}\right)^{\frac{1}{2}} \frac{(1+\alpha M_i)^{\frac{1}{2}}}{M_i} , \tag{1}$$

where for magnetic flux compression ($\gamma = 2$)

$$p_i = p_f (r_f/r_i)^2 \tag{2}$$

is the initial pressure of the payload and $\alpha \approx 1.5$ is a phenomenological constant. For thick liners the final pressure achieved is given by

$$\zeta_f^{(1)} = p_f/\rho c^2 = M_i (1+\alpha M_i). \tag{3}$$

3

By replacing Eq. (2) with the two-dimensional form,

$$p_i = p_f (r_f/r_i)^4 \tag{4}$$

we can define the compression efficiency for an equivalent cylindrical geometry according to

$$\epsilon^{(1)} = \frac{\pi r_f^2 p_f}{(2\pi r_i d_i)(\tfrac{1}{2}\rho u_i^2)} = \frac{2\zeta_f}{M_i^2 b_f^2} \tag{5}$$

where $b_f^2 = 2r_i d_i/r_f^2$ is the ratio of the initial cross-sectional area of the liner to that of the final payload volume. Substitution of (3) in (5) yields

$$\epsilon^{(1)} = \frac{2(1 + \alpha M_i)}{b_f^2 M_i} . \tag{6}$$

The efficiency cannot exceed unity, of course; as $M_i \to 0$, Eq. (6) must go over to $\epsilon = 1$ (the incompressible result). In the high Mach number case, i.e., when $\zeta_f \ll b_f^2 M_i^2 (1+\alpha M_i)^{-\frac{1}{2}}$, Eq. (3) is replaced by

$$\zeta_f = M_i(1+\alpha M_i)(d_i/d^*)^2 \approx \tfrac{1}{4} M_i b_f^2 \tag{7}$$

whence from (5)

$$\epsilon^{(1)} = (2M_i)^{-1} \tag{8}$$

Somon and Jablon [11] extended these results to the case of supersonic ($M_i \gg 1$) cylindrical liners. Their numerical simulations showed that the maximum pressure is given by

$$\zeta_f \approx 1.1 b_f^{0.89} M_i^2 \tag{9}$$

4

and hence the compression efficiency is

$$\epsilon^{(2)} \approx 3.8 \ (M_i^2/\zeta_f)^{1.25} \approx 3.3 \ b_f^{-1.11}. \qquad (10)$$

Other quantities of interest can be found from ζ_f and Eq. (4).

Robson[12] applied the concept of the effective liner thickness to cylindrical geometry for the low Mach number case and final pressures $\zeta_f \leqslant 0.05$. The results are rather insensitive to the choice of the "effective outer radius" r^*. They show that the ratio of p_f to p_o, the final pressure the liner would reach if it were incompressible, is a decreasing function of both ζ_o and b_o (parameters defined analogously to ζ_f and b_f using p_o instead of p_f and r_o, the incompressible final state radius, instead of r_f). Our results in the present paper, which are restricted to $\zeta_f \geqslant 0.05$ for numerical reasons discussed below, appear to be roughly consistent with Robson's.

Schaffer, using the same equation of state and the same fluid equations of motion (except for the absence of rotation) as ours, performed a series of numerical experiments using an implicit finite-difference algorithm. He found[13] that a good fit to the results could be expressed in the form

$$\epsilon \approx [1 + \zeta_f(b_f/F)^2]^{-\frac{1}{2}} \qquad (11)$$

where

$$F/4.8 = \begin{cases} 1 & b_f \leqslant 20 \\ 1+0.65 \ \ell n(b_f/20) & b_f > 20. \end{cases} \qquad (12)$$

Over a considerable range of the parameters the effective radius r^* satisfied $r^*/r_f \approx 26$.

In order to understand better the effects of compressibility and to develop scaling laws of a nature sufficiently general to aid in designing and interpreting liquid liner experiments[14], we have adopted the following simple model (cf. Fig. 1). A cylindrical liner is described using the Euler equation for the radial aximuthal velocity components, together with the equation of state given by Somon[9]. Both liner surfaces are assumed to be free. The pressure

5

at the inner surface is derived from the adiabatic law for the payload

$$p_1 = p_0 \left(r_0 / r_1 \right)^{2\gamma} , \qquad\qquad (13)$$

where γ is the adiabatic index (usually taken to be $5/3$) and p_1 is
the pressure at the inner radius r_1. The outer pressure is taken to
be constant (specifically, zero for the calculations reported here).

Thus the liner and plasma are taken to behave as ideal fluids (no
energy dissipation or other loss mechanisms are modeled).
By neglecting the driving pressure and the boundary conditions
appropriate to realistic driving pistons, we greatly reduce the
complexity of the model, without lessening its applicability to
the part of the trajectory in the immediate vicinity of turnaround.
As in all liner implosion problems, the most interesting effects
which we wish to concentrate on are observed only near turnaround
anyway. The liner rotation is then chosen in such a fashion that
the criterion for rotational stabilization of Rayleigh-Taylor modes
on the inner surface is marginally satisfied during the implosion:

$$g = \frac{d^2 r_1}{dt^2} - \frac{v_1^2}{r_1} \leq 0, \qquad\qquad (14)$$

where v_1 is the azimuthal velocity at the inner surface. [It turns
out that the maximum in $g(t)$ always occurs just prior to turnaround,
where equality therefore holds in Eq. (14).]

Using this model, we initialize the liner trajectory at some
point shortly before turnaround and solve the equations of motion in
finite-differenced form to find the behavior of the liner as a
function of time. The fractions of total energy at turnaround in
the form of payload compression, rotation, liner internal energy and
radial kinetic energy,   the value of Q, and the amplitude of the
pressure pulse at the outer radius are found for various initial
conditions. The results are summarized in the form of plots versus

6

ζ_f and M_∞, the limiting form of u_1/c at asymptotically large radius, then crossplotted to reveal their dependence on effective driving pressure and compression ratio.

The plan of this paper is as follows. In Section II we review the dynamics of incompressible liners, then recast the problem in dimensionless variables. The numerical techniques used are described in considerable detail, especially the way in which knowledge of the incompressible dynamics is used to initialize the calculations. The results of the calculations are then presented in Section III, with particular attention to the wave effects (water hammer and dwell enhancement) mentioned above. We summarize our conclusions in Section IV.

II. Formulation of the Problem

A. Review of Incompressible Liner Dynamics

We begin our treatment of compressibility effects in imploding cylindrical liquid liners by reviewing the most important features of the motion of incompressible liners. Although the latter constitute an idealization quite unattainable in operating regimes of reactor interest, their study is valuable for two reasons. First, they are easier to analyze, and for some purposes the effects of compressibility can be ignored (but it is important to know when they cannot). Second, at sufficiently large radii any freely imploding or expanding liner behaves as if it is incompressible. Therefore, the entire dynamic trajectory can be specified simply by writing down the parameters which specify its asymptotic incompressible form.

As Somon[15] has shown, given the equations of state of liner and payload, two dimensionless parameters are required for this purpose in the absence of rotation. Inclusion of an arbitrary free vortex rotation (azimuthal velocity inversely proportional to radius) increases the number to three. That is, any physical quantity q associated with a particular liner trajectory is determined as a function of time according to a law of the form

$$q = \tilde{q}\,[t\,;\,p_1,\,p_2,\,p_3;\,S_1,\,S_2,\,S_3], \qquad (15)$$

where the p_i are dimensionless parameters labeling the trajectory, and the S_i are dimensionless quantities which set the scales of length, time and mass.

For an incompressible liner it is natural to choose as scale factors the liner density ρ, the minimum inside radius r_o, and the radial "velocity at infinity" u_∞. The latter is the uniform coasting speed approached in the absence of external pressure at radii so large that the liner is thin and the back pressure of the compressed payload and the dynamic pressure within the liner resulting from cylindrical convergence are negligible. The dimensionless parameters are conveniently chosen as b, the ratio of liner thickness to inner radius at turnaround; Ω_o, the angular velocity of the inner surface at turnaround, scaled by u_∞/r_o; and P_o, the payload pressure p_o at turnaround, divided by ρu_∞^2. The zero of time is either taken as the instant of turnaround, or as the time when we begin following the trajectory, in which case turnaround occurs at $t = t_o$. (Throughout this paper, the zero subscript denotes quantities associated with incompressible liner motion, evaluated at turnaround. The corresponding values for compressible liners are labeled with the subscript f, for "final.") This choice of dimensionless parameters and scale factors has the advantage of relating the dynamical trajectory to the properties of the system at turnaround, i.e., those which determine the thermonuclear properties of the system. It may, however, not be optimum for purposes of experimental design.

The equation of motion is the radial component of the force law,

$$\rho\left(\frac{\partial u}{\partial t} + u\frac{\partial u}{\partial r} - \frac{v^2}{r}\right) + \frac{\partial p}{\partial r} = 0, \qquad (16)$$

where u and v are the radial and azimuthal components of velocity and p is the pressure. Conservation of angular momentum is expressed by the azimuthal component of the force law,

8

$$\frac{\partial v}{\partial t} + u \frac{\partial v}{\partial r} + \frac{uv}{r} = 0. \qquad (17)$$

The equation of state is the condition of incompressibility,

$$\frac{1}{r} \frac{\partial}{\partial r} (ru) = 0 \qquad (18)$$

By virtue of (18), the radial velocity field in the liner is inversely proportional to r,

$$u(r,t) = r_1(t) \, u_1(t)/r \qquad (19)$$

(subscripts 1 and 2 label quantities associated with the inner and outer surfaces of the liner, respectively), and the area between the inner radius and a radial displacement comoving with a liner fluid element is a constant,

$$r^2 - r_1^2 = r^2(0) - r_1^2(0). \qquad (20)$$

Solution of (17) yields the result that v is a linear combination of a free vortex and a rigid body rotation. We omit the latter for simplicity (this is a good approximation if the liner, which starts from a state of rigid rotation, is thin at that time). The azimuthal velocity field of the liner can now be written

$$v(r,t) = \Omega_o u_\infty \, r_o/r. \qquad (21)$$

Substitution of (19) and (21) in (16) enables us to calculate the pressure profile

$$p(r,t) = p_1 + [p_2 - p_1 - \delta p \, (1 - r_1^2/r_2^2)] \, \ell n(r^2/r_1^2)$$

$$/ \, \ell n(r_2^2/r_1^2) + \delta p \, (1 - r_1^2/r^2), \qquad (22)$$

9

where

$$\delta p = \frac{1}{2} \rho \ (u_1^{\ 2} + v_1^{\ 2}).\qquad\qquad (23)$$

The pressure p_2 on the outer surface is assumed to vanish, so that
we do not have to model the mechanism that produces the implosion.
With   this external pressure is in
fact negligible for all states in the vicinity of turnaround.
Equation (22) has a maximum at $r = r_m$, defined by

$$\frac{r_m^{\ 2}}{r_1^{\ 2}} = \frac{\delta p \ \ell n(r_2^{\ 2}/r_1^{\ 2})}{p_1 + \delta p \ (1-r_1^{\ 2}/r_2^{\ 2})} \qquad\qquad (24)$$

When δp is sufficiently large, $r_1 < r_m < r_2$, and there is a maximum
in the pressure across the liner; then the slope of the pressure at
$r = r_1$ is positive. From Eq. (16), this means that the net accel-
eration (inertial minus centrifugal) on the inner surface,

$$g = \frac{d^2 r_1}{dt^2} - \frac{v_1^{\ 2}}{r_1} , \qquad\qquad (25)$$

is negative. This is the criterion for rotational stabilization of
Rayleigh-Taylor modes on the inner surface[7]. If at some time the
slope of $p(r)$ turns negative at $r = r_1$, the motion becomes unstable.

    To estimate how large the maximum pressure $p(r_m)$ is, we can sub-
stitute Eq. (24) in Eq. (22) with $p_2 = 0$. The resulting expression
simplifies if we assume $(r_1/r_2)^2 \ll (r_m/r_2)^2 \ll 1$, whereupon

$$p(r_m) \approx p_1 + \delta p = p_{max}. \qquad\qquad (26)$$

Evidently, we can have pressure peaks in the interior of the liner
which exceed p_1 by a considerable amount.

    We assume that the energy is conserved (no losses take place
through magnetic diffusion, streaming out the ends, etc.). The
pressure of the compressed payload, and therefore p_1, satisfies an

10

adiabatic law

$$p_1(t) = P_0 \, \rho u_\infty^2 \, (r_0'/r_1)^{2\gamma}, \tag{27}$$

with ratio of specific heats γ satisfying $5/3 \leq \gamma \leq 2$. This corresponds to a payload varying between pure ideal gas or plasma ($\gamma = 5/3$) and pure axial magnetic flux ($\gamma = 2$). By virtue of Eqs. (19-22) and (26) it is possible to specify the implosion dynamics totally once $r_1(t)$ is known. An equation for r_1 can now be written in the form

$$(R\ddot{R} + \dot{R}^2) \, \ell n(1 + b^2/R^2) = (R^2\dot{R}^2 + \Omega_0^2) \, b^2/(R^2 + b^2)$$

$$+ 2 \, P_0 R^{-2\gamma}, \tag{28}$$

where $R = r_1/r_0$ and the dots denote differentiation with respect to the dimensionless time $\tau = u_\infty t/r_0$. The integral of Eq. (28) is

$$(R^2\dot{R}^2 + \Omega_0^2) \, \ell n(1+b^2/R^2) + 2P_0 R^{2(1-\gamma)} /(\gamma-1) = b^2. \tag{29}$$

This is the dimensionless form of the statement of the conservation of energy,

$$W_{kin} + W_{rot} + W_{pay} = W_{tot}, \tag{30}$$

where

$$W_{tot} = \tfrac{1}{2} \, \pi \, \rho \, b^2 \, u_\infty^2 \, r_0^2$$

is the total energy per unit length, and

$$W_{kin} = \tfrac{1}{2} \, \pi \, \rho \, u_\infty^2 \, R^2\dot{R}^2 \, \ell n \, (1+b^2/R^2), \tag{31}$$

$$W_{rot} = \tfrac{1}{2} \, \pi \, \rho \, u_\infty^2 \, \ell n \, (1+b^2/R^2), \tag{32}$$

and

$$W_{pay} = \frac{\pi\rho u_\infty^2}{\gamma-1} \, P_0 R^{2(1-\gamma)} \tag{33}$$

11

are the radial, rotational and payload energies, respectively, per unit length.

At turnaround $(\tau = \tau_o = u_\infty t_o/r_o)$, $R = 1$ and $\dot{R} = 0$, and we have from Eq. (29)

$$\Omega_o^2 \ln(1+b^2) + \frac{2P_o}{\gamma-1} = b^2. \qquad (34)$$

The compression efficiency is

$$\epsilon = W_{pay}/W_{tot} = \frac{2P_o}{(\gamma-1)b^2} . \qquad (35)$$

We can specify Ω_o by demanding that at turnaround the system be **marginally** stabilized against Rayleigh-Taylor modes by rotation. The condition for this to occur is that Eq. (14) vanish at $t = t_o$, i.e.,

$$\ddot{R}(t_o) = \Omega_o^2. \qquad (36)$$

It is easy to see that if Eq. (36) holds at turnaround, $g < 0$ for all $r_1 > r_o$. Substituting Eq. (36) in Eq. (28) with $R = 1$ yields

$$\Omega_o^2 \left[\ln(1+b^2) - b^2/(1+b^2)\right] = 2P_o. \qquad (37).$$

Now Eq. (35) becomes

$$\epsilon = \left[1 + \frac{(\gamma-1)\ \ln(1+b^2)}{\ln(1+b^2) - b^2/(1+b^2)}\right]^{-1}. \qquad (38)$$

Note that P_o also has dropped out of this expression for ϵ; this result, that the compression efficiency depends only on b, is characteristic of incompressible liner dynamics [16].

In the thin liner limit $b \rightarrow 0$, the condition for rotational stabilization becomes harder to satisfy, and ϵ vanishes as b^2. The efficiency increases monotonically with b, and in the thick liner limit $(b \rightarrow \infty)$, ϵ approaches γ^{-1}. Practically speaking, this

12

limit is attained when $b \gtrsim 20$. The fraction of the total energy tied up in rotation in a stabilized liner, $\delta = 1 - \gamma^{-1}$, is ~50% even for thick liners.

B. Compressible Dynamics

The most obvious qualitative effect of compressibility is a reduction of the payload compression achieved at the time of turn-around, defined by $dr_1/dt = 0$. For a given compressible liner trajectory, asymptotically identical at large radii to that of an incompressible liner of the same dimensions, radial and angular velocity and density, the minimum radius actually reached will be larger, $r_f > r_o$. Some of the energy that would have gone into payload compression goes instead into compressing liner material. At the same time, some energy will be tied up in the radial motion of the outer portion of the liner, since a finite interval comparable with the transit time of sound is required to communicate the information that the inner surface has stopped. In the energy conservation equation, which now takes the form

$$W_{kin} + W_{rot} + W_{pay} + W_{int} = W_{tot}, \qquad (39)$$

where W_{int} is the energy which goes into compressing liner material, all the terms on the left hand side are in general non-vanishing at turnaround.

An additional class of phenomena is associated with compressional waves propagating in the liner. The most dramatic is the "water hammer," an abrupt pressure peak which is followed by a rarefaction, both expanding radially outward following turnaround. Depending on the external boundary conditions, it can reflect back in and execute several transits during the expansion phase of the liner. Closely related to the water hammer is an effect we term "dwell enhancement". For an incompressible liner, $r_1(t)$ is symmetric about $t = t_o$, and the dwell time t_d, arbitrarily defined as the length of time during which $r_1 \leq 2r_o$, is exactly bisected by

13

turnaround. When compressibility is accounted for, the liner is seen to recede from the turning point more slowly then it approached. It is in effect tamped by the still-imploding outer portion, and cannot expand freely until the rarefaction wave reflected from the outer surface reaches the inner surface.

To model compressibility in liquid metals realistically, we use instead of Eq. (18) an equation of state previously employed by Somon[15]

$$p = \bar{p} \left(\frac{\rho}{\rho}\right)^2 \left(\frac{\rho}{\rho} - 1\right). \tag{40}$$

Properly speaking, p should have an additional term which depends on entropy through the temperature T. By adopting the isentropic form ($\bar{p}$ and $\bar{\rho}$ constant), we relinquish any prospect of correctly describing shocks, in return for a considerable simplification of the numerical analysis. (This point will be further discussed below.) Equation (40) implies that the compressional energy density is quadratic in ρ. The corresponding bulk modulus of compression $B = \rho \frac{dp}{d\rho}$ can be written

$$B(p) = B_o + B_o' \, \rho, \tag{41}$$

where $B_o' = 3$ and $B_o = \rho^2$ is weakly dependent on p in the regime of moderate compression. That is, Eq. (40) is approximately equivalent to a Grüneisen equation [3] with coefficient $B_o' = 3$.

By thus assuming that all fluid elements have the same entropy and the same specific angular momentum $A = rv$ at all times, we can combine Eqs. (16), (19) and (40) in the form

$$\frac{\partial u}{\partial t} + u \frac{\partial u}{\partial r} - \frac{A^2}{r^3} + \frac{\bar{p}}{\bar{\rho}} \left(3 \frac{\rho}{\bar{\rho}} - 2\right)\frac{1}{\rho} \frac{\partial \rho}{\partial r} = 0. \tag{42}$$

We also need the continuity equation,

$$\frac{\partial \rho}{\partial t} + \frac{1}{r} \frac{\partial}{\partial r} (r\rho u) = 0. \tag{43}$$

14

Equations (42) and (43) can be used to advance u and ρ, with all the other fluid quantities derived from these. The boundary conditions are as before, Eq. (27) and $p_2 = 0$.

It is useful to write Eqs. (42) and (43) in dimensionless form, using for this purpose the uncompressed density $\bar{\rho}$, the speed of sound in the liner at zero pressure, c, defined by

$$c^2 = \bar{p}/\bar{\rho}, \tag{44}$$

and some approximation for the final radius r_f. Since r_f is not known <u>a priori</u>, but only as a result of propagating Eqs. (42) and (43), we begin by scaling with r_o instead. Both are unambiguously determined by specifying the dynamic trajectory, but r_o has no simple relation to r_f. Thus we write

$$u' = u/c; \tag{45}$$
$$r' = r/r_o; \tag{46}$$
$$t' = ct/r_o; \tag{47}$$
$$\rho' = \rho/\bar{\rho}; \tag{48}$$

and

$$\omega_o = A/(r_o c). \tag{49}$$

Now we have the equation

$$\frac{\partial \rho'}{\partial t'} + \frac{1}{r'} \frac{\partial}{\partial r'} (r'\rho'u') = 0; \tag{50}$$

$$\frac{\partial}{\partial t'} (\rho'u') + \frac{1}{r'} \frac{\partial}{\partial r'}(r'\rho'u'^2) +$$

$$+ \frac{\partial}{\partial r'} \left[\tfrac{1}{2} \omega_o^2/r'^2 + (\tfrac{3}{2} \rho' - 2) \rho' \right] = 0, \tag{51}$$

where Eq. (51) has been rewritten in conservative form. These are the basic equations of our model, the numerical solution of which provides the basis for the present paper. Henceforth, it is under-

15

stood that we are working with the reduced variables defined in Eqs. (45-49), and the primes will be omitted:

$$\frac{\partial \rho}{\partial t} + \frac{1}{r} \frac{\partial}{\partial r} (r \rho u) = 0; \qquad (52)$$

$$\frac{\partial}{\partial t} (\rho u) - \frac{1}{r} \frac{\partial}{\partial r} (r \rho u^2) + \frac{\partial}{\partial r} [\frac{1}{2} \omega_o^2/r^2 + (\frac{3}{2} \rho - 2)\rho] = 0. \qquad (53)$$

We now imagine that a liner has imploded to some radius $r_1 = r_i$, where at time $t = 0$ we begin following it by means of Eqs. (52-53). At some earlier time, for radii $r_1 \gg r_i$, the liner must certainly have behaved incompressibly, and we can characterize its trajectory by specifying b, Ω_o and P_o, as before. Anticipating the importance of compressibility effects, however, we employ instead the three parameters M, ω_o and ζ_o, where

$$M = u_\infty/c, \qquad (54)$$

$$\omega_o = M \Omega_o, \qquad (55)$$

and

$$\zeta_o = P_o/M^2. \qquad (56)$$

The incompressible thickness b can be derived from the new trajectory parameters by Eq. (34), which now becomes

$$\omega_o^2 \ln (1+b^2) + 2\zeta_o/(\gamma-1) = b^2 M^2. \qquad (57)$$

The reason for switching from b as a trajectory label is that at $t = 0$, when we initialize, the liner must already have become somewhat compressed [remember that, as shown by Eq. (26), the pressures within the liner may become large long before p_1 does]. Ignoring this and taking $r_2^2 - r_1^2$ to be the same as its asymptotic value would increase the mass of the liner [according to Eq. (40)] by an amount dependent on the choice of r_i. Under the circumstances b, defined as the ratio of two quantities which no longer have a simple

16

interpretation in terms of observables, becomes dispensable.

The parameters ω_o and ζ_o are still open to the objection that their definition involves quantities associated with the final radius reached by an incompressible liner. Therefore, once we have found the minimum radius r_f actually reached, we make a final replacement, introducing in their stead the parameters ω_f and ζ_f, defined by

$$\omega_f = v_f/c = \omega_o/a_f \tag{58}$$

and

$$\zeta_f = p_f/\bar{\rho}\, c^2 = \zeta_o\, a_f^{-2\gamma}, \tag{59}$$

where

$$a_f = r_f/r_o \tag{60}$$

Clearly, ω_f and ζ_f, although defined only implicitly through numerical integration of (52) and (53), are characteristic of the trajectory and, together with M, specify it completely.

C. Numerical Treatment

At $t = 0$, we expect the functions $u(r)$, $v(r)$ and $p(r)$ to be almost the same as they would be for an incompressible liner. [Otherwise, we have chosen a starting point too close to turnaround.] Yet, as we have seen, this form of $p(r)$ is inconsistent with a constant density ρ when we adopt the equation of state (40). For reasons to be discussed shortly, it is impractical to choose r_i so large that the discrepancy is negligible. Instead, we proceed as follows. Write

$$u(r,0) = u^{(0)}(r) + u^{(1)}(r), \tag{61}$$

where

$$u^{(0)}(r) = r_1\dot{r}_1'/r \tag{62}$$

and we have assumed that

$$|u^{(1)}(r)| \ll |u^{(0)}(r)|. \tag{63}$$

17

Here $\dot{r}'_1$ is a constant to be determined. Substituting (61) in
Eq. (53) and dropping first order terms yields

$$\frac{r_1\ddot{r}'_1 + \dot{r}'^2_1}{r} - \frac{r_1^2\dot{r}'^2_1 + \omega_o^2}{r^3} + \frac{\partial}{\partial r}\left[\rho\left(\frac{3}{2}\,\rho - 2\right)\right] = 0, \qquad (64)$$

where $\ddot{r}'_1$ is a second undefined constant. Integration results in a
quadratic for $\rho(r)$:

$$\rho\left(\frac{3}{2}\,\rho - 2\right) - \frac{1}{2}\left[(r_1\ddot{r}'_1 + \dot{r}'_1)^2 \,\ell n\,(r^2/r_1^2)\right.$$

$$+ (r_1^2\dot{r}'^2_1 + \omega_o^2)(r_1^{-2} - r^{-2})] = -\frac{1}{2}\,[1$$

$$+ (r_1\ddot{r}'_1 + \dot{r}'^2_1)\,\ell n\,(r'^2_2/r_1^2) + (r_1^2\,\dot{r}'^2_1$$

$$+ \omega_o^2)\,(r_1^{-2} - r'^{-2}_2)], \qquad (65)$$

where r'_2 is a third undefined constant. [Note that $\rho = 1$ at
$r = r'_2$ in (65) as a result of the choice of the integration con-
stant.]

The three unknowns $\dot{r}'_1$, $\ddot{r}'_1$ and r'_2 are the velocity and radial
acceleration at the inner surface, and the radius of the outer sur-
face, respectively. They are chosen by requiring that the pressure
at $r = r_1$ have the correct value

$$\zeta_1 = p_1/\bar{\rho}c^2 = \zeta_o r_1^{-2\gamma} \qquad (66)$$

and by requiring that the total liner mass (and therefore the angular
momentum) and the total system energy have the same values as "at
infinity:"

$$2\int_{r_1}^{r'_2} r\,dr\,\rho(r) = b^2, \qquad (67)$$

18

$$\int_{r_1}^{r_2'} r\,dr\,\rho(r)[(r_1^2\dot{r}_1'^2 + \omega_o^2)/r + (\rho-1)^2]$$
$$+ \frac{2\zeta_o r_1^{2(1-\gamma)}}{\gamma-1} = b^2 M^2. \tag{68}$$

Equations (66-68) were solved by a version of Newton's method, using the incompressible values of $\dot{r}_1$, $\ddot{r}_1$ and r_2 as the starting point.

The first order correction $u^{(1)}$ can be obtained from Eq. (52):

$$\frac{1}{r}\frac{\delta}{\delta r}(ru^{(1)}) = -(\frac{\delta\rho}{\delta t} + u^{(o)}\frac{\delta\rho}{\delta r})/\rho \tag{69}$$

where the time derivative on the right hand side has to be obtained by differentiating the implicit time dependence of r_1. Similarly, first order corrections to ρ can be obtained from Eq. (53). The procedure is very involved, and in any case cannot be expected to yield a convergent expansion. Fortunately, there is no need to go beyond lowest order.

In operation the initialization was completed by specifying M, ω_o, ζ_o, and a starting value of the inner radius r_i. The solutions were propagated in time and the function $g(t)$ was monitored until u_1 became positive, then ζ_o was incremented by some preassigned value $\delta\zeta_o$ and the whole process repeated. After the minimum of $g(t)$ (including only times after the grid ringing had ceased) became negative, the loop on ζ_o was restarted with a smaller increment $\delta\zeta_o$. When three-place accuracy had been attained in the crossing value, the system was considered to be marginally stable, and a final run was carried out through the expansion phase (out to some maximum radius $r_1 \sim 5\text{-}10\ r_f$) for the purpose of calculating water hammer pressure histories and the total thermonuclear yield. The latter was calculated according to the following formula[17] for a 50-50 D-T mixture ($n_D = n_T = 0.5n$) as

$$P_{DT} = 4.3\ n^2\ T^{-\frac{2}{3}}\ \exp(-19.94\ T^{-\frac{1}{3}})\,\text{erg/cm}^3 \tag{70}$$

where T is in keV, and both n and T are supposed to vary adiabatically. Each calculation integrated Eq. (70) for 50 different

starting values of T, and Q was determined using the one which gave the biggest yield. Note that the numerical coefficient in (70) is larger than that given in ref.(17) by $(5.0/3.68)(22.4/17.6)=1.73$. The first factor arises from optimizing the theoretical fit to the experimental cross-section in the energy range $T \lesssim 25$ keV, and the second results from taking account of the energy produced by tritium breeding in the lithium component of the liner.

As we are interested in the compressional waves which can propagate through the liner, our code, called WAVER, used a time-centered <u>explicit</u> finite difference technique to solve Eqs. (52-53) numerically. An implicit technique would correctly describe the gross features of the implosion, at the same time relaxing the Courant-Friedrichs-Lewy[18] (CFL) timestep condition so that the code could run up to two orders of magnitude faster, but it would not be accurate in describing wave propagation unless the time steps were shortened and made comparable to the CFL limit. Because of the steepness of the water hammer pressure pulse, ETBFCT,[19] a vectorized continuously rezonable flux-corrected transport[20] module, was utilized in Lagrangian mode. Satisfactory results were obtained even on runs of 10,000 to 20,000 timesteps, provided r_i was taken to be of order 5-10 times the final radius r_f. If r_i was larger than this, however, grid point bunching occurred, resulting in inordinately short timesteps and unphysical profiles.

The grid was laid down initially so that the spacing would have become uniform if the liner had imploded incompressibly to the origin. This prescription yielded a closely gridded region near r_1 and large spacing near r_2, as desired. Grid point bunching was alleviated somewhat by filtering the flow velocity when it was used to advance the grid points (but not in advancing the fluid equations):

$$r_j^{n+1} = r_j^n + \tilde{u}_j^{n+\frac{1}{2}} \delta t, \tag{71}$$

where $\tilde{u}_j$ was calculated using the finite-differenced form of

$$\tilde{u} = u + \frac{1}{r}\frac{\partial}{\partial r}\left(Dr\frac{\partial u}{\partial r}\right). \tag{72}$$

20

The best results were obtained with $D = 0.5(\delta r)^2$, where δr is the
(variable) mesh spacing. Use of $\tilde{u}_j$ instead of u_j also greatly
reduced oscillations in the grid motions. This is particularly
important in the neighborhood of $r = r_1$, because the finite-
difference form of the acceleration of the inner surface [Eq. (25)]
was monitored as a stability diagnostic. At the outset of the
calculation $g(t)$ displayed drastic "ringing" in these grid points
for all but the thickest liners. This was attributed to discrepan-
cies between the initial profiles used and the exact solutions they
approximated. The ringing (which showed up in g but not in r_1 or
$\dot{r}_1$) damped away quickly, whereupon g varied smoothly until after
turnaround, when ringing again ensued.

Aside from the high frequency oscillations superposed on g,
which were clearly of numerical origin, all the results were sub-
stantially independent of the number of mesh points, chosen to vary
between 25 and 200, and the choice of r_i, except as noted above.
The number of mesh points was usually taken to be the largest number
which would permit running all the cases with a given value of M
in $\sim$ 10,000 cycles or less.

Conservation of mass and angular momentum were built into the
code, and were satisfied to within roundoff, but conservation of
energy was subject to truncation error. Up to turnaround, W_{tot}
was constant to $\leq 2\%$ in all cases. After the water hammer was
launched, however, W_{tot} decreased by as much as 10-15%. This was
attributed to entropy production, that is, to the tendency of the
outgoing wave to steepen and form a shock. As noted above, our
equation of state is isentropic and cannot describe shocks. In
spite of this, we feel that the overall wave motion is calculated
approximately correctly, until it reflects off the free surface of
the outer radius.

We have dealt with the numerical techniques we used and the
problems associated with them in unusually fine detail for two
reasons. First, the use of an explicit code to solve compressible
fluid equation in the nearly incompressible limit is very difficult,

and the answers obtained need to be examined critically. Second, we have developed no analytical theory which reproduces the systematic content of our results, and consequently cannot resort to theory to check or corroborate them. In spite of this, on the basis of considerable effort spent in code development and numerical tests, we feel confident in their accuracy.

III. Numerical Results

A. Energetics

Using the techniques described in the previous section for the "slow to intermediate" range of liner speeds, $M = 0.01 - 0.2$, we obtained the results shown in Figs. 2-5. Curves are plotted for five cases, denoted by A through E. Cases A-D have a payload gas with $\gamma = 5/3$, and $M = 0.2$, 0.1, 0.05 and 0.01, respectively, while for case E, $\gamma = 2$ and $M = 0.1$. The broken portions of the traces represent interpolations between the calculation and the incompressible $(\zeta_f=0)$ limit, in the range where the explicit finite difference methods used become erratic or prohibitively expensive. The remainder of the curves (solid traces) are smooth fits through the numerical results.

Figure 2 shows that, except for $M \ll 1$ (case D) and $\zeta_f \ll 1$, the fraction of energy residing in liner internal compression is roughly independent of M, ζ_f and γ. A single curve fits almost all the points well; the flat part corresponds to $W_{int}/W_{tot} \approx 0.15$. As $\zeta_f \to 0$, the liners get thinner, the pressure profiles across them become flatter, and $W_{int}/W_{tot} \to 0$. This requires the continuation (broken trace) to turn down as shown. For $\zeta_f < 0.05$, the values so obtained agree to within a factor of two with those calculated by Robson[12].

Case D evidently disproves the universality of this curve and suggests the existence of a nontrivial dependence on M. There seems to be little need to pin this down, however, as all points on curve D but the ones with $\zeta_f < 0.1$ refer to extraordinary thick liners $(b/a_f \gtrsim 500$; see Fig. 8 below).

A reduction in payload compression efficiency of order 15% or less due to liner compressibility is quite acceptable. However, this is not the whole story. The radial (translational) portion of the kinetic energy is considerably larger and increases with both M and ζ_f. Together, W_{int} and W_{rad} amount to about half of W_{tot} when $\zeta_f \gtrsim 0.5$. In neither plot does the dependence on γ (represented by the differences between cases B and E) appear very significant. For experimentally realizable payloads consisting of a mixture of plasma and flux, the effective value of γ can be taken constant, approximately equal to 1.8[21].

Figure 4 shows that the fraction of the total energy required for rotational stabilization decreases as ζ_f increases. All of the traces have been extended to intercept the ordinate at $1-\gamma^{-1}$, corresponding to the intercepts at γ^{-1} in Fig. 5. This is in accord with the discussion following Eq. (38) above, where it was noted that for an incompressible liner, $W_{rot}/W_{pay} \to \gamma-1$ in the thick-liner limit. Of course, $\zeta_f = 0$ refers to a liner of infinitesimal thickness, for which $\epsilon=0$ and $\delta = W_{rot}/W_{tot} = 1$. The crossover ($b \sim 1$) to the thin-liner case occurs at such low final pressures, however, that no error is made for finite ζ_f in ignoring it. Practically speaking, all liners of interest are thick at turnaround.

Because of the γ-dependence in the incompressible limit, cases B and E are necessarily different at low ζ_f. It is seen from Fig. 4 that they also differ for larger ζ_f. The dependence on M is also quite noticeable. Evidently there is an energetic penalty for going to fast implosions ascribable to both the radial and rotational components of the kinetic energy.

In all cases, marginal stability occurred before turnaround. The net acceleration $g(t)$ [Eq. (25)] always climbed to a maximum, then dropped away as compressibility effects flattened the shape of the trajectory $r(t)$, reducing d^2r/dt^2. Because the difference between the inertial and centrifugal terms in g is not a strong function of radius near turnaround, the relation between ζ_f, b and ω_f (the amount of rotation needed for marginal stabilization) is almost the

same as that for incompressible liners, Eq. 34. The discrepancy was $\leq 5\%$ for all cases with $b \leq 100$, that is, roughly speaking, for $M > 0.01$ and $\zeta_f \leq 0.3$.

Figure 5 shows the compression efficiency $\epsilon = W_{pay}/W_{tot}$ as a function of M and ζ_f. The curves drop off with increasing ζ_f very sharply at first, then more smoothly. Efficiency improves with increasing M, varying by a factor of ~ 3 for a given value of ζ_f over the range of Mach numbers investigated. The efficiency is significantly greater for $\gamma = 5/3$ then for $\gamma = 2$, the difference being approximately twice the incompressible value of 20% for most of the range of ζ_f.

If we plot ϵ^{-1} against M and ζ_f, the results can be closely fitted by straight lines through the incompressible intercept. Thus we have as a good approximation

$$\epsilon^{-1} = \gamma[1 + h(M/\gamma)\zeta_f], \qquad (73)$$

where h is evidently an decreasing function of M and an increasing function of γ [cf.Eq. (11) in the Introduction, the fit obtained by Schaffer for a non-rotating liner.] We have no adequate model to explain this simple dependence on ζ_f, but the following heuristic argument may at least make it plausible.

As we have seen, treating the effects of compressibility changes W_{int} and W_{rot} only slightly from the values found for incompressible liners, and the changes have opposite signs. Hence $W_{pay} + W_{rad}$ is roughly the same in both cases, and we can modify the thick-liner limit of Eq. (38) to read

$$\frac{W_{pay} + W_{rad}}{W_{tot}} = \frac{1}{\gamma} , \qquad (74)$$

or

$$\epsilon^{-1} = \frac{W_{tot}}{W_{pay}} = \frac{\gamma(W_{pay} + W_{rad})}{W_{pay}} . \qquad (75)$$

24

As we noted in the Introduction, the finite speed of sound makes the liner act as though only a portion with outer radius $r^* < r_2$ is effective in compressing the payload. Thus Eq. (75) can be written

$$\epsilon^{-1} = \frac{\gamma \, \ell n \, (r_2{}^2/r_f{}^2)}{\ell n \, (r^{*2}/r_f{}^2)} \, , \tag{76}$$

where

$$r^* = r_f + K_1 ct. \tag{77}$$

Here t is the dwell time of the liner,

$$t = K_2 r_f/u_{eff}, \tag{78}$$

K_1 and K_2 are factors of order unity, and the effective velocity u_{eff} is determined from expression (31) for the radial kinetic energy by

$$u_{eff}{}^2 = \frac{2 \, W_{rad}}{\pi \rho r_1{}^2 \, \ell n \, (r_2{}^2/r_1{}^2)} \approx \frac{2 \, W_{rad}}{\pi \rho r_f{}^2 \, \ell n \, (r_2{}^2/r_f{}^2)} \tag{79}$$

Hence by (75)

$$u_{eff}{}^2 = \frac{2 \, W_{pay} \, (1-\epsilon\gamma)}{\epsilon\gamma \, \pi \, r_1{}^2 \rho \, \ell n \, (r_2{}^2/r_f{}^2)}$$

$$\approx c^2 \, \frac{2 \, \zeta_f}{\gamma(\gamma-1) \, \epsilon \, \ell n \, (r_2{}^2/r_f{}^2)} \tag{80}$$

Combining Eqs. (76-78) and (80) in the limit of large ζ_f, where $r^* - r_f << r_f$, there results

$$\epsilon^{-1} = \frac{\gamma}{2K_1 K_2 (\gamma-1)} \, \ell n \, (r_2{}^2/r_f{}^2) \, \zeta_f \tag{81}$$

While r_2/r_f does depend on ζ_f, the dependence in ϵ^{-1} is logarithmically weaker and can be omitted. Interpolation between Eq. (81) and the $\zeta_f \rightarrow 0$ limit $\epsilon^{-1} = \gamma$ now yields the desired form (73).

25

Turning to the question of thermonuclear efficiency, we calculate the yield from Eq. (70) according to

$$Y = \int_{-\infty}^{\infty} dt \, P_{DT}(t) \, \pi \, r_1^2(t). \tag{82}$$

[The actual limits of the integral are from $t = 0$ to approximately the time when the calculation stops, i.e., when r_1 is 1 to 2 times $r_1(0)$.] Using the fact [22] that P_{DT}/T^2 is practically constant as a function of temperature, we rewrite Eq. (82) in the form

$$Y = \rho^2 \, c^3 \, r_f \int cdt/r_f \, (nT/\rho c^2)^2 (P_{DT}/T^2)\pi \, r_1^2/n^2. \tag{83}$$

The $Q = Y/W_{tot}$ is given by

$$Q = \rho c \, r_f \, (2/b_f^2 M^2) \int cdt/r_f \, (nT/\rho c^2)^2 (P_{DT}/T^2)(r_1/nr_f)^2, \tag{84}$$

where the right hand side is a scaling factor $\rho c r_f$ multiplying an expression which depends only on dimensionless trajectory parameters.

In Fig. (7), $Q/\rho c r_f$ is plotted against ζ_f for the cases A-D defined previously. It is significant that, although Q increases noticeably with M, there is no dependence to speak of on ζ_f. This may seem surprising in view of the results of Fig. 5, which showed that relatively little energy gets into the payload for large ζ_f. The explanation lies in the fact that the dwell period, when $r_1 \sim r_f$ and P_{DT} is near its maximum, is extended due to tamping of the inner portion of the liner by the outer portion. Figure 8 shows how this makes $r_1(t)$ much flatter during the rebound. The resulting enhancement in the thermonuclear burn, which is quadratic in T, is even more pronounced. The beneficial and adverse effects of liner compressibility appear in this sense roughly to cancel.

Another dimensionless parameter which can be used in place of M to characterize the liner trajectory is the radial compression ratio $\alpha_f = r_1(0)/r_f$. For a liquid liner driven by pistons, high efficiency

26

dictates that there should be as little fluid as possible in the form of an initial buffer layer on the chamber wall and in the ducts after the piston stroke is finished. To the extent this is achieved, then, we can set

$$r_1(0) \approx r_2(t_f) \approx r_w, \tag{85}$$

where r_w is the radius of the chamber. Thus

$$\alpha_f \approx r_2(t_f)/r_f \approx b_f. \tag{86}$$

Figure 9 displays computed values of α_f (i.e., b_f) as a function of ζ_f and M for cases A-D. Note that the requirement of rotational stabilization results in very thick ($b_f > 100$) liners for all pressures except $\zeta_f \lesssim 0.1$ when M = 0.05.

Using Fig. 9 to determine M as a function of α_f and ζ_f enables us to plot $Q/\rho c r_f$ vs. the latter quantities (Fig. 10). For a fixed compression ratio, Q vanishes as $\zeta_f \rightarrow 0$. Q increases rapidly at first, then slowly. For a given final pressure ζ_f, Q is a decreasing function of α_f; at large ζ_f, however, this dependence is weak.

From Fig. 10, it is evident that the thermonuclear gain increases monotonically with increasing relative payload pressure ζ_f. The basic hydrodynamic results for compressible liquid liner implosions thus do not <u>by themselves</u> indicate an optimum operating value from ζ_f. At fixed compression ratio, higher values of ζ_f appear to lead to smaller values of r_f for desired thermonuclear gains, i.e., to smaller system sizes. The total system size, however, will depend not only on the outer radius of the liner, $\alpha_f r_f$, but also on the thickness of the pressure vessel required to contain the liquid liner during implosion and reexpansion. In an idealized way, this consideration of the engineering requirements of the system will increase the total system radius by a factor $(1 + p_D/S)$, where p_D is the peak pressure of the gas driving the liner implosion and S is the allowable mechanical stress. The peak pressure will depend on the particular driving mechanism but can be scaled by the work

27

done at constant pressure to obtain the desired payload pressure:

$$p_D = K \frac{\zeta_f \rho c^2}{(\gamma-1)\alpha_f^2} \cdot \frac{1}{\epsilon(\zeta_f, \alpha_f)} , \qquad (87)$$

where K is a proportionality constant to account for nonconstant driving pressure during the implosion. The total radius r_T, of the system may then be estimated as

$$r_T = r_f \alpha_f (1 + p_D/S) = r_f \alpha_f (1 + \Sigma^* \zeta_f / \epsilon \alpha_f^2) \qquad (88)$$

where $\Sigma^* = \lambda \frac{\rho c^2}{S}$ is a parameter based on the properties of the liner, payload and drive mechanism, and $\lambda = K/(\gamma-1)$.

The results of Fig. 10 can be used to obtain r_T for a desired value of Q in terms of mechanical properties and the peak payload pressure ζ_f, for fixed values of α_f. In Fig. 11, we plot $(\lambda c/S)Q/r_T$ versus ζ_f for $\alpha_f = 30$ and two values of $\Sigma^* = 50$ and 600, (corresponding roughly to constant pressure drive with sodium-potassium and lead liners, respectively, and a mechanical stress of about 10^8 Pa). A clear maximum is evident for $\Sigma^* = 600$, occurring at $\zeta_f = 0.1$, while for $\Sigma^* = 50$ the maximum is broader and occurs at about $\zeta_f = 0.45$. Dividing the scaled values for Q_p displayed in Fig. 11 by $\epsilon(\zeta_f)$, scaled values for the thermonuclear energy gain Q_p relative to the peak plasma energy may be obtained as shown in Fig. 12. Note that, as expected, the optimum operating points shift to higher values of ζ_f. For a "scientific feasibility" experiment, defined as $Q_p = 1$, with $\alpha_f = 30$ and $\Sigma^* = 600$, the idealized total system radius is found by dividing the scaled Q_p value at $\zeta_f = 0.2$ into $\lambda c/S$. If $c = 1.6 \times 10^5$ cm/sec, $\lambda = 1.5$, and $S = 7.3 \times 10^8$ dyne/cm^2 (10,000 psi), then the necessary total radius is $r_T = 29$ cm. Magnetic diffusion at the inside surface of the liner, finite effective beta values for the payload, and practical engineering design considerations will, of course, increase the system size. The present calculations are merely to indicate the manner in which the optimum operating value of ζ_f can be determined.

28

B. Water Hammer

Figure (13) shows the development of the water hammer in a rotating compressible liquid liner. We observe that the pressure profile displays the characteristic internal maximum. Just after turnaround (Fig. 13c), the payload pressure has begun to drop from its maximum ($\zeta_f \approx 0.5$) and a rarefaction is developing. The rarefaction broadens, while the front of the pulse (the water hammer proper) at $r = r_{max}$ steepens (Figs. 13d, e). These processes continue until the water hammer reaches the outside of the liner. There the free surface boundary condition ($p_2 = p(r_2) = 0$) forces the pulse to reflect as a rarefaction, and the calculation is no longer physically meaningful.

We can, however, cancel out the spurious effects of the free-surface boundary condition sufficiently to estimate the radial sidewall pressure produced when the pulse reaches a solid boundary. We do this by noting that as the pulse propagates toward r_2, the value of the pressure approaches a $1/r$ dependence increasingly closely. Thus, writing

$$p_w = p_{max} r_{max}/r_2, \tag{89}$$

and plotting p_w for successive instants until r_{max} is a few mesh points away from r_2, we find a number which does not depend on the conditions near $r = r_2$. The dimensionless form of p_w, namely $\zeta_w = p_w/\rho c^2$, is plotted in Fig. 14 against ζ_f and M for cases A-C. We observe that although the curves increase monotonically with ζ_f, they become quite flat for large values, especially in case C. In general, ζ_w/ζ_f is a sizeable fraction (typically $\sim \frac{1}{5}$) for small ζ_f. Serious attention must be given to design of the experimental apparatus in order that it be able to tolerate such loads.

Of even greater importance is the force on the endwalls, since they must be built so as to permit access to the chamber and therefore contain holes or other structures. Figure 15 displays $\Theta(\zeta_f, M)$, the dimensionless peak endwall thrust, calculated according to

29

$$\Theta \rho c^2 \pi \, r_f^2 = 2\pi \int_{r_1}^{r_2} p(r) \, r dr \qquad (90)$$

for the same cases A-C. Maximum Θ naturally always occurs just as the water hammer reaches the outside of the liner; as may be seen from Fig. 15, it increases strongly with ζ_f for ζ_f large, unlike the sidewall pressure ζ_w. Furthermore, Θ is largest for small Mach numbers, reflecting the scaling by πr_f^2. The peak endwall pressure loading per unit outside circumference, Θ/α_f, to a good approximation is independent of M.

IV. Discussion

We have calculated three related but distinct effects of finite compressibility in rotationally stabilized, cylindrical liquid liners. These are the reduction in compression ratio, enhancement of the dwell stage (and correspondingly, of the thermonuclear yield), and the water-hammer-induced pressure loading on endwalls and side-walls. The calculations span the region of M-$\dot{\zeta}_f$ parameter space describing conditions which must be attained in a fusion reactor and which are achievable by imploding thick liners. The results are embodied in the plots presented in Section III, especially Figs. 5-7, 9-12 and 14-15.

These results are correct in detail only for a system satisfying our model assumptions, namely, cylindrical symmetry, no dissipation mechanisms, and a payload of pure plasma. Changing these assumptions can affect the results in two ways. First, as we have seen in the discussion of the allowable total stress, the introduction of more realistic assumptions can select an operating point for the system, or at least define a region in parameter space which is most favorable from the standpoint of the new considerations. Second, new physical assumptions can change the curves themselves. For example, inclusion of radiation, end losses, thermal conduction, etc., in the plasma model reduces both the plasma compression efficiency and the value of Q.

To the extent that such losses are small, we can represent them by multiplicative efficiency factors. Thus the effects of magnetic diffusion into the liner, incursion of liner vapor impurities into the plasma, and the existence of a nearly plasma-free region of magnetic flux within the payload volume can all be represented in a single geometric factor ϵ_f. We say that the payload energy W_{pay} is distributed roughly uniformly through a region of radius $r_f^{(2)} = r_f + \Delta_2$, where Δ_2 is the magnetic skin depth. Within this region the plasma occupies a volume of effective radius $r_f^{(1)} = r_f - \Delta_1$, where Δ_1 is a layer of impurities and buffer field. Then the energy in the plasma is

$$W_{p1} \approx W_{pay}[(r_f - \Delta_1)^2 / (r_f + \Delta_2)^2]$$

$$\approx W_{pay}[1-2(\Delta_1 + \Delta_2)/r_f] = \epsilon_f W_{pay}. \qquad (91)$$

Simularly, W_{dr}, the driving energy from the source, is converted by the pistons into the total liner energy W_{tot} with an efficiency

$$\epsilon_m = W_{tot} / W_{dr} \qquad (92)$$

Hence the actual thermonuclear efficiency with inclusion of these loss mechanisms is

$$Q' = Y/W_{dr} = Y/(W_{p1} / \epsilon_m \epsilon_c \epsilon_f)$$

$$= \epsilon_m \epsilon_c \epsilon_f Q_p = \epsilon_m \epsilon_f Q \qquad (93)$$

where ϵ_c and Q are the compression efficiency (Fig. 5) and thermonuclear efficiency (Fig. 6) computed in this paper.

The present work represents a completed stage of a continuing theoretical program in support of the Linus concept. It will be followed by calculations to be presented in a later paper, in which the inefficiencies referred to in the definition of ϵ_f — specifically, magnetic diffusion and finite plasma beta — are treated

31

self-consistently along with compressibility. Our eventual
objective is the realization of the inherently favorable character-
istics afforded by controlled liner implosion in the design and demon-
stration of a viable reactor configuration.

Acknowledgements

We wish to thank Mrs. Peggy Thume for her efforts in preparing
this manuscript for publication, and Dr. M. J. Schaffer for dis-
cussing the results of his calculations with us in advance of
publication. Discussion with Dr. A. E. Robson of the results of
our calculations is also acknowledged. This work was supported by
the Office of Naval Research and The Energy Research and Development
Administration.

33

References

1. D. L. Book, A. L. Cooper, R. Ford, D. A. Hammer, D. J. Jenkins, A. E. Robson and P. J. Turchi, *Plasma Physics and Controlled Nuclear Fusion Research 1976*, Vol. III, p. 507 (Proc. VI International Conference on Plasma Physics and Controlled Nuclear Fusion Research, Berchtesgaden, FGR, 6-13 October 1976, IAEA, Vienna, 1977).

2. C. M. Fowler, W. B. Garn and R. S. Caird, J. Appl. Phys 31, 588 (1960).

3. H. Knoepfel and F. Herlach, Eds., *Megagauss Magnetic Field Generation by Explosives and Related Experiments*, EUR 2750.e (Euratom, Brussels, 1960).

4. A. D. Sakharov, R. Z. Lyudaev, E. N. Smirnov, Yu. I. Plyuschev, A. J. Pavlovskii, V. K. Chernyshev, E. A. Feoktistova, E. I. Zharinov and Yu. A. Zysin, Dokl. Akad. Nauk SSSR 165, 65 (1965) [Sov. Phys. Dokl 10, 1045 (1966)].

5. S. G. Alikhanov, V. G. Belan, G. I. Budker, A. I. Ivanchenko and O. N. Kichigin, At. Energia 23, 536 (1967) [Sov. J. At. Energy 23, 1307 (1967)].

6. D. L. Book and N. K. Winsor, Phys. Fluids 17, 662 (1974); A. Barcilon, D. L. Book and A. L. Cooper, Phys. Fluids 17, 1707 (1974).

7. P. J. Turchi, A. L. Cooper, R. Ford, and D. J. Jenkins, Phys. Rev. Lett. 36, 1546 (1976).

8. H. Knoepfel, *Pulsed High Magnetic Fields* (American Elsevier, New York, 1970), Chapt. 10.

9. J. P. Somon, "L'Equation d'Etat des Solides," LGI Rept 64/3 (1964).

10. G. Lehner, J. G. Linhart and J. P. Somon, Nucl. Fus. 4, 362 (1964).

11. J. P. Somon and C. Jablon, Nucl. Fus. 16, 1040 (1976).

12. A. E. Robson, NRL Memorandum Report No. 3472 (1977).

13. M. J. Schaffer (to be published).

14. P. J. Turchi, Proc. Seventh Symposium on Engineering Problems of Fusion Research, Knoxville, Tenn., 25-28 Oct. 1977.

15. J. P. Somon, J. Fluid Mech. $\underline{38}$, 769 (1969); Ref. 3, p. 67.

16. A. Barcilon, D. L. Book, J. P. Boris, A. L. Cooper, K. Hain, P. C. Liewer, A. E. Robson, R. A. Shanny, P. J. Turchi and N. K. Winsor, Plasma Physics and Controlled Nuclear Fusion Research 1974, Vol. II, p. 567 (Proc. V International Conference on Plasma Physics and Controlled Nuclear Fusion Research, Tokyo, 11-15 November 1974, IAEA, Vienna, 1975).

17. Samuel Glasstone and R. H. Lovberg, Controlled Thermonuclear Reactions (Krieger Publ. Co., Huntington, N. Y., 1975), pp. 20-23.

18. R. Courant, K. O. Friedrichs, and H. Lewy, Mathematische Annalen $\underline{100}$, 32 (1928) [transl. IBM Journal, March, 1967, pp. 215-234.]

19. J. P. Boris, NRL Memorandum Report No. 3237 (1976).

20. J. P. Boris and D. L. Book, in Methods in Computational Physics, Vol. 16, ed. by John Killeen, [Academic Press, New York, 1976], p. 85.

21. D. L. Book, D. A. Hammer and P. J. Turchi, Nucl. Fus. $\underline{18}$, 000 (1978).

22. J. W. Shearer and W. C. Condit, in Energy Storage, Compression and Switching, Ed. W. H. Bostick, V. Nardi and O. S. F. Zucker (Plenum Press, New York, 1976), p. 109.
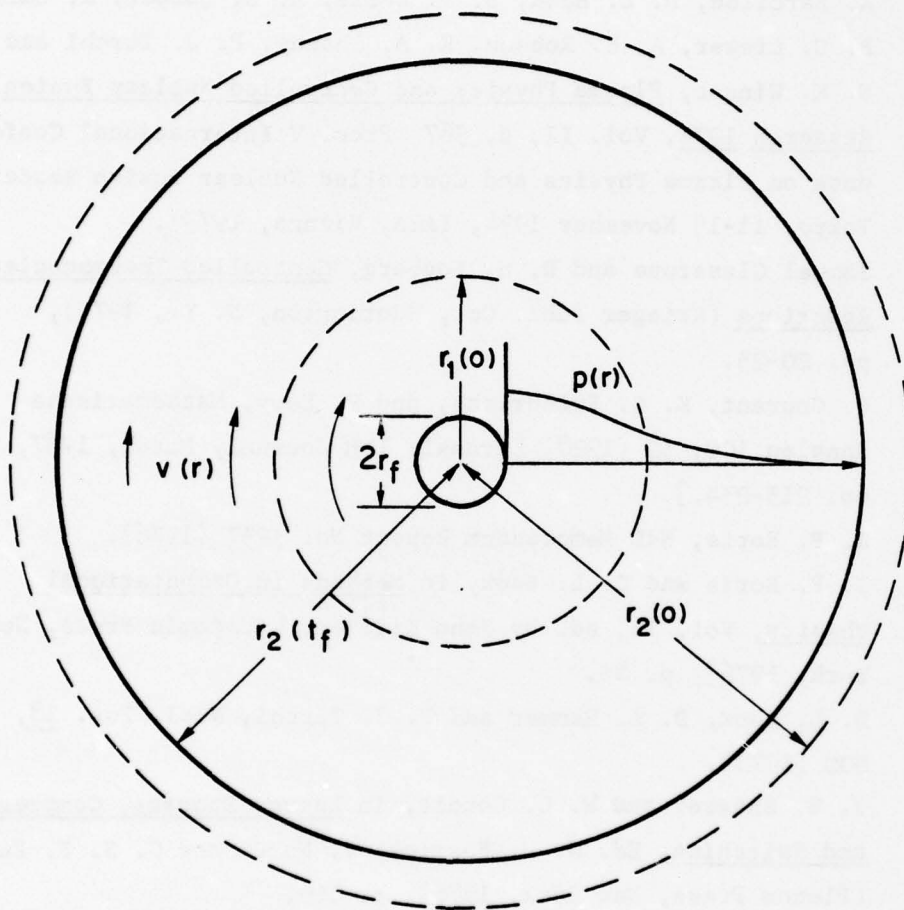
Fig. 1 — Schematic of model used. At some time t = 0 the liner has inner and outer radii $r_1(0)$ and $r_2(0)$, respectively corresponding to the dashed circles. At turnaround, these become $r_1(t_o) = r_f$ and $r_2(t_o)$ (solid circles). For a stable implosion, pressure profiles $p(r)$ are qualitatively as shown. Azimuthal velocity $v(r)$ decreases as $1/r$.
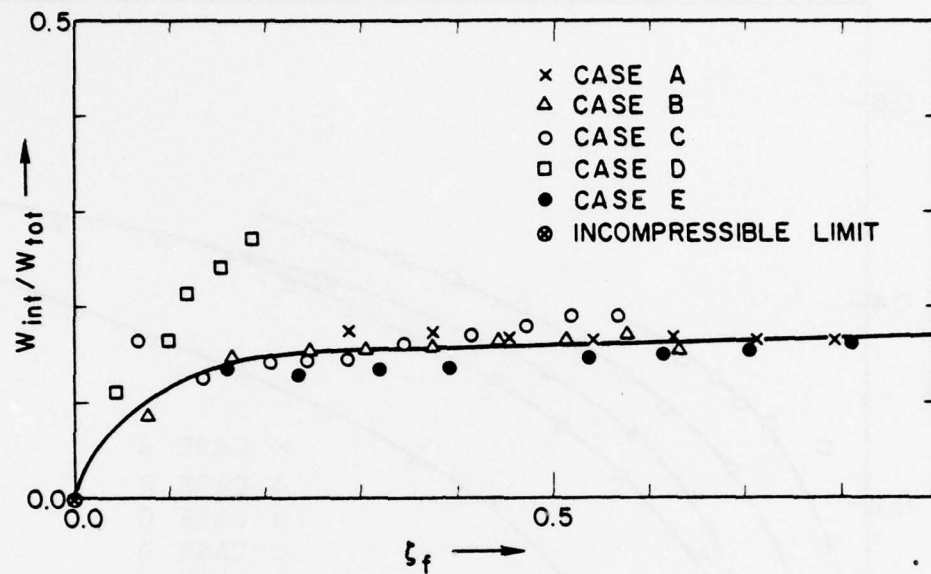
Fig. 2 — Ratio of internal (compressional) liner energy to total energy at turnaround as a function of dimensionless final pressure ζ_f, for several choices of M and γ. All cases are marginally stable against Rayleigh-Taylor modes. As $\zeta_f \to 0$, $W_{int} \to 0$ (no liner compression).
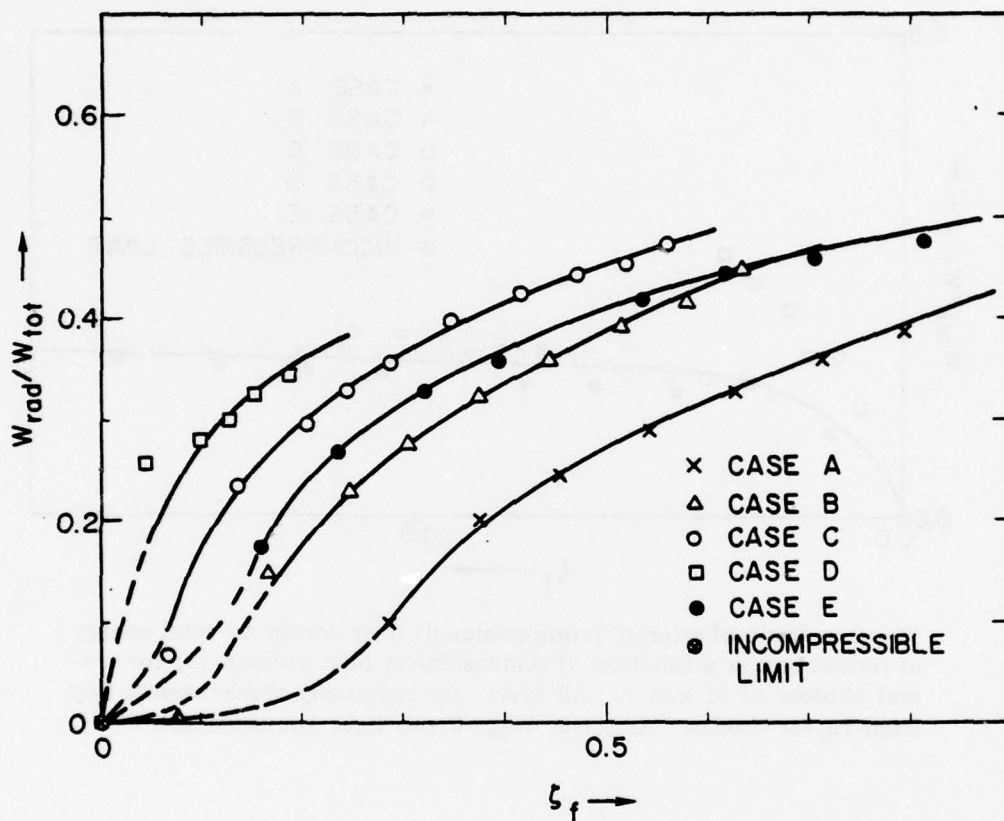
Fig. 3 — Ratio at turnaround of radial kinetic to total energy vs ζ_f for the same cases as in Fig. 2. Broken curves indicate extrapolation of numerical results to the incompressible limit.

38
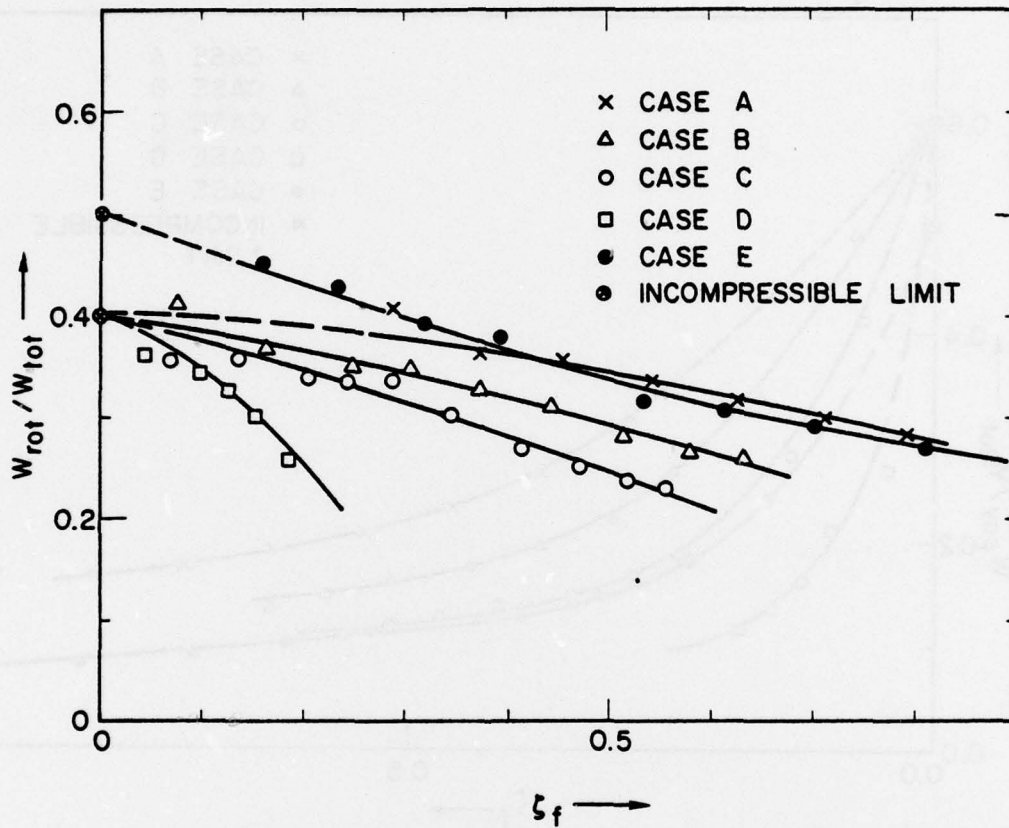
Fig. 4 — Ratio at turnaround of rotational kinetic to total energy vs ζ_f for same cases as in Figs. 2-3. Note that the $\gamma = 2$ incompressible limit differs from that of the $\gamma = 5/3$ cases.
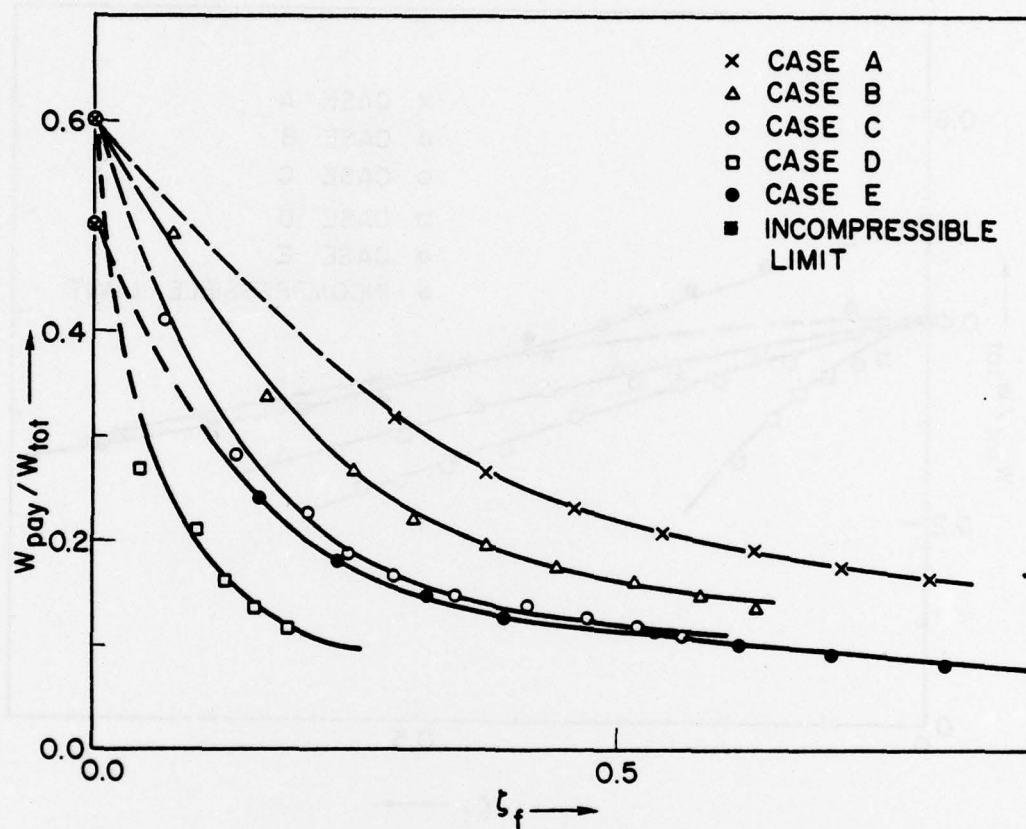
Fig. 5 — Ratio of payload (compressed plasma/flux configuration) to total energy vs. ζ_f for same cases as in Figs. 2-4
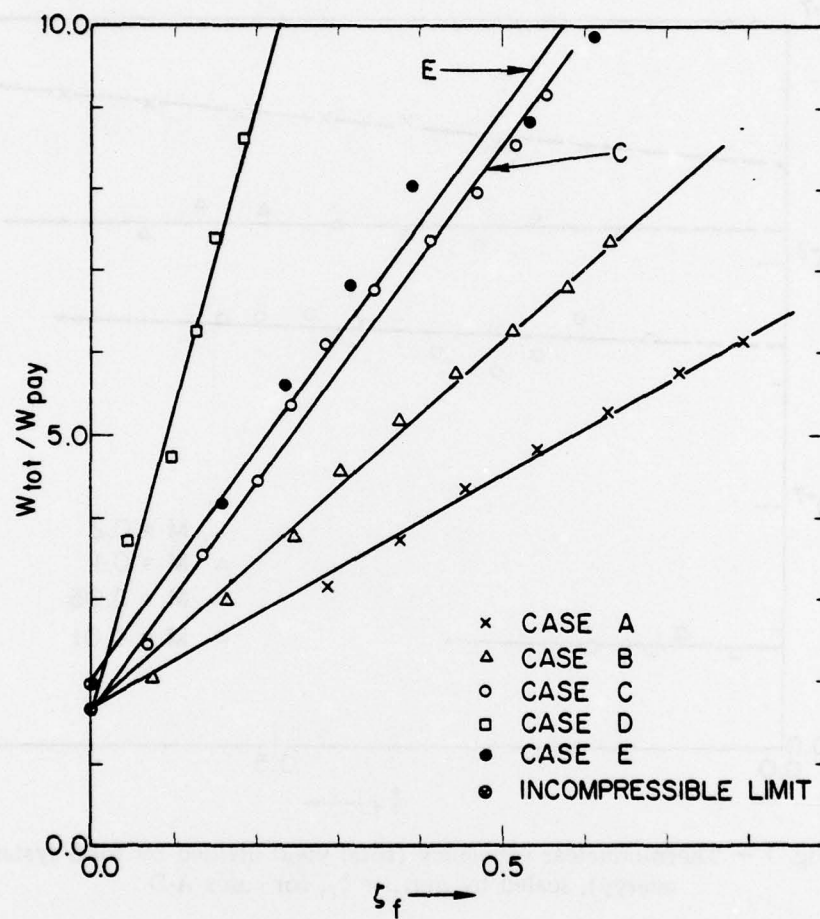
Fig. 6 — Ratio of total energy to payload energy (inverse of quantity plotted in Fig. 5) vs ζ, showing straight-line fits

41
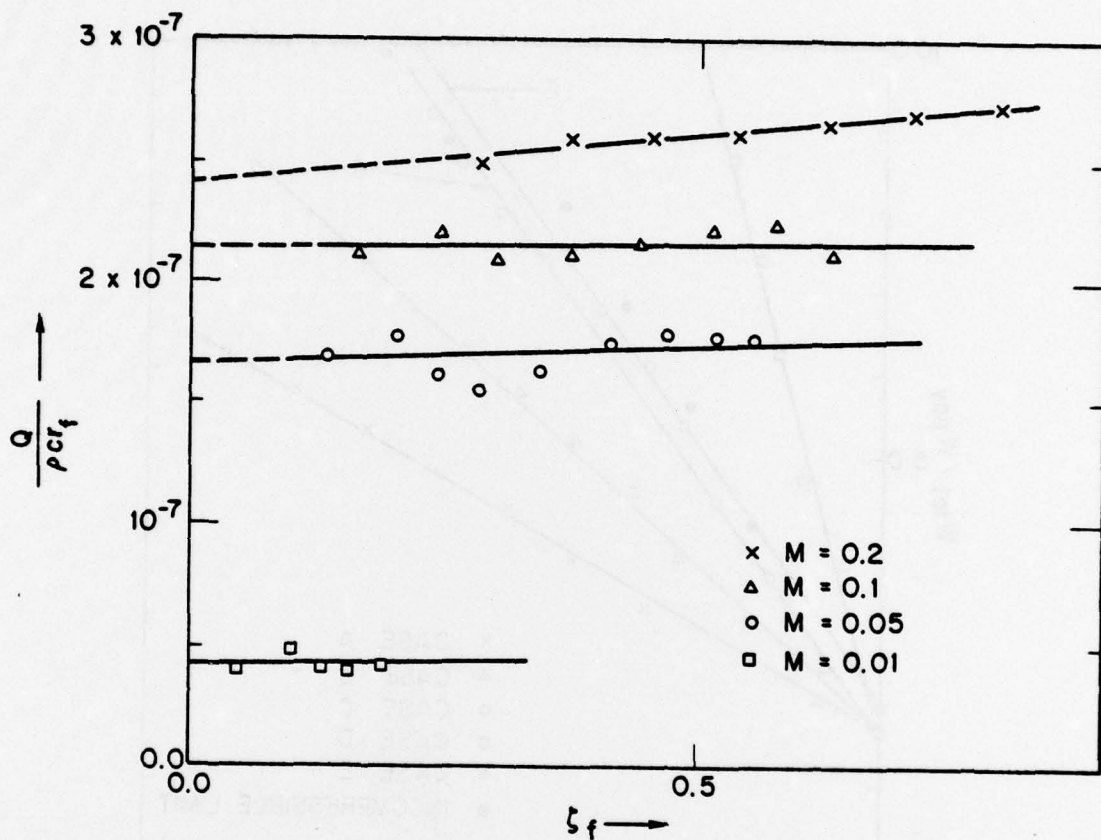
Fig. 7 — Thermonuclear efficiency (total yield divided by total system energy), scaled by $\rho c r_f$, vs ζ_f, for cases A-D
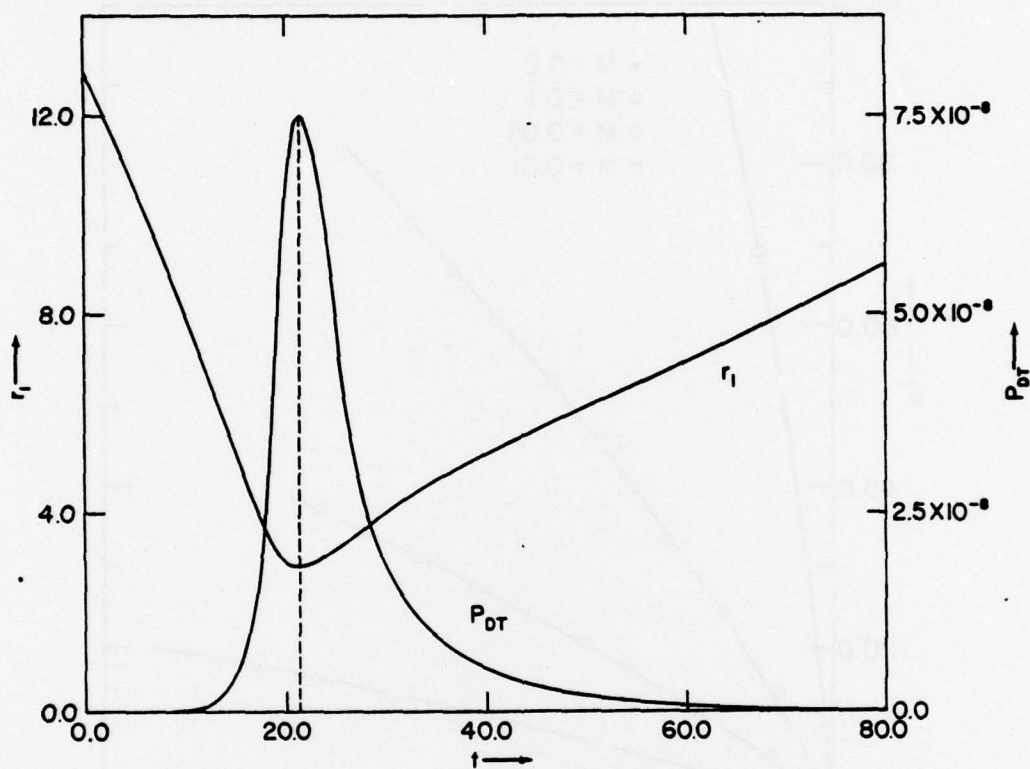
Fig. 8 — Liner inner radius r_1 and thermonuclear power output per unit length $\overline{P}_{DT}$ vs time for a strongly compressed case ($M = 0.2$, $\zeta_f = 0.794$). The units of radial displacement and time are r_o and c/r_o, where r_o is the radius which would be reached by the liner if it were incompressible; $\overline{P}_{DT}$ is measured in units of $\rho c^2 r_o^2$. The asymmetry in $r_1(t)$ near turnaround (dwell enhancement) causes a substantial increase in P_{DT} after turnaround.

43
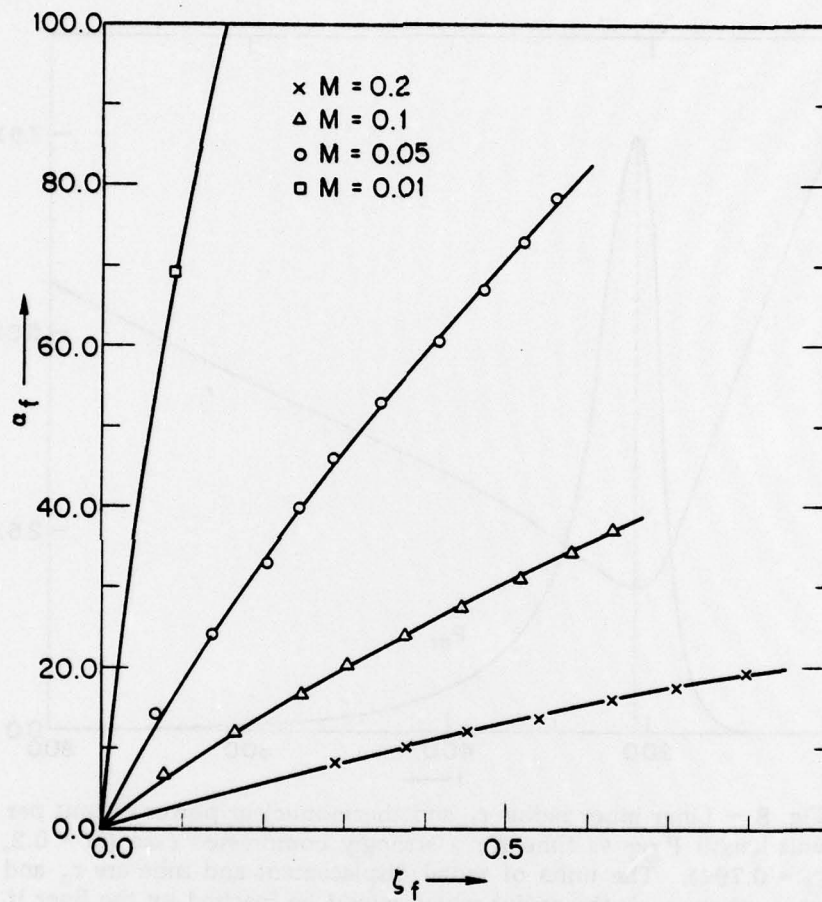
Fig. 9 — Radial compression ratio a_f (liner thickness at turnaround scaled by r_f) vs ζ_f for cases A-D

44
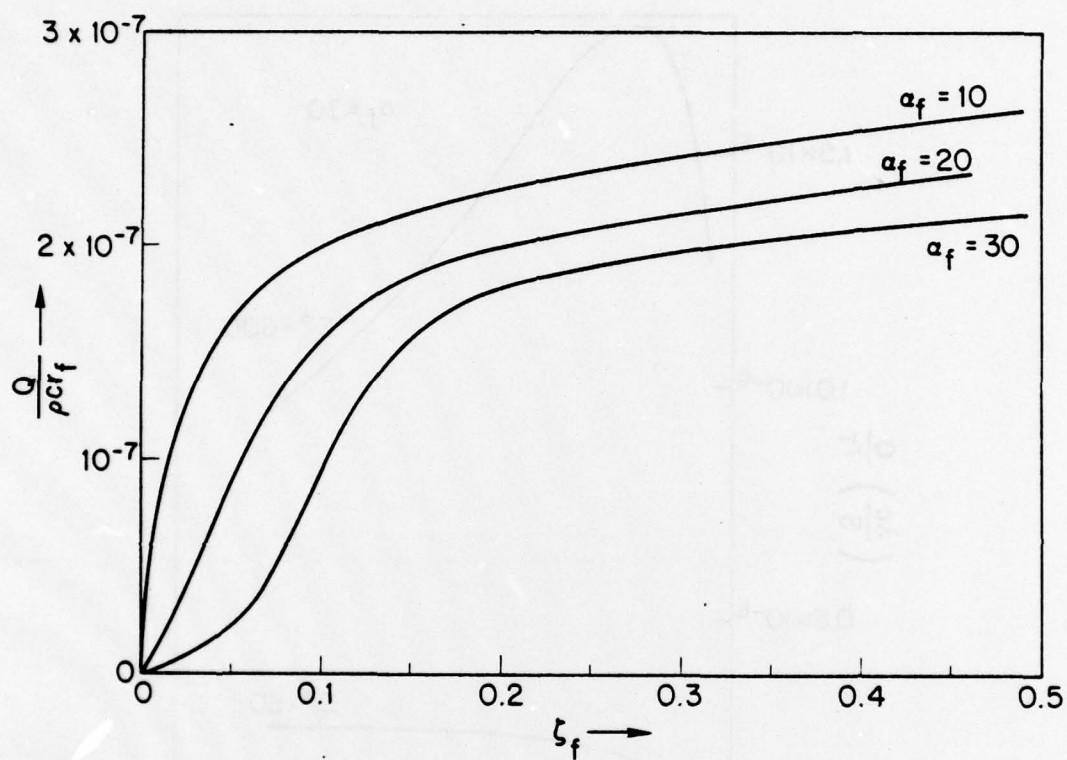
Fig. 10 — $Q/\rho c r_f$ vs ζ_f for fixed α_f
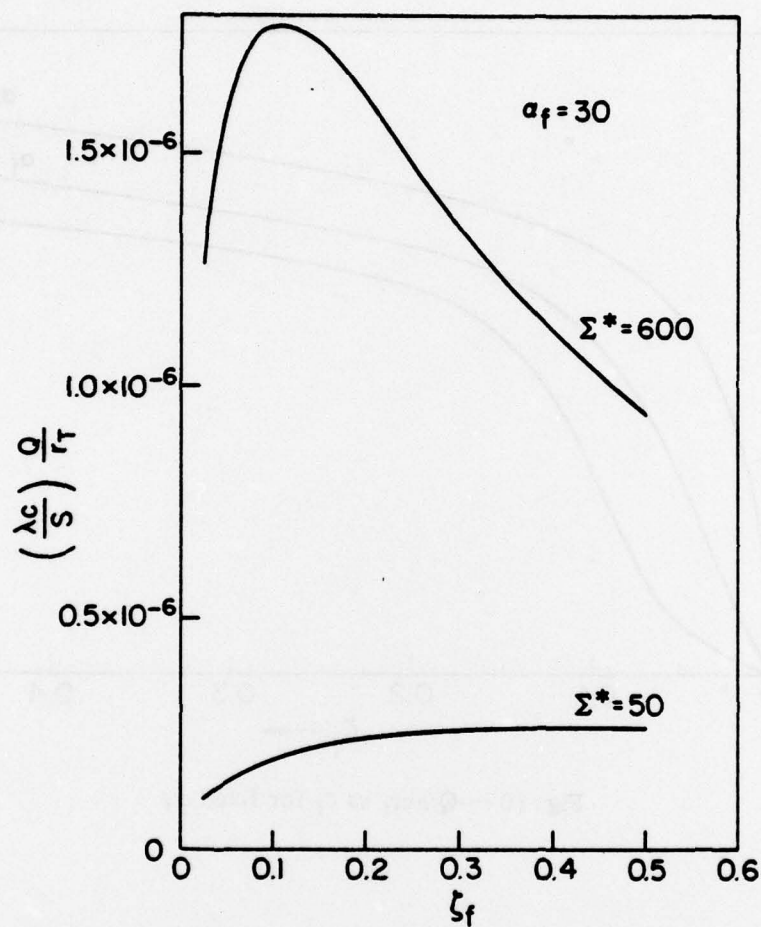
Fig. 11 — Plots of Q (scaled by $Sr_T/\lambda c$ instead of $\rho c r_f$) vs ζ_f
for $\alpha_f = 30$ and $\Sigma^* = 50, 600$

46
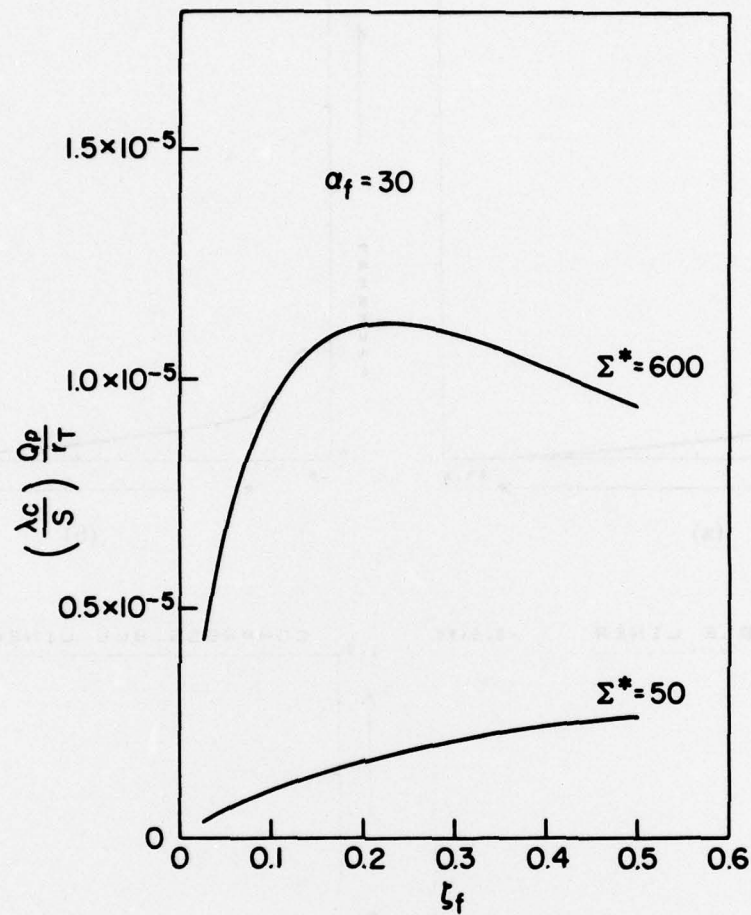
Fig. 12 — As in Fig. 11: $Q_p = Q/\epsilon$, scaled by $Sr_T/\lambda c$, vs ζ_f for $\alpha_f = 30$ and $\Sigma^* = 50, 600$
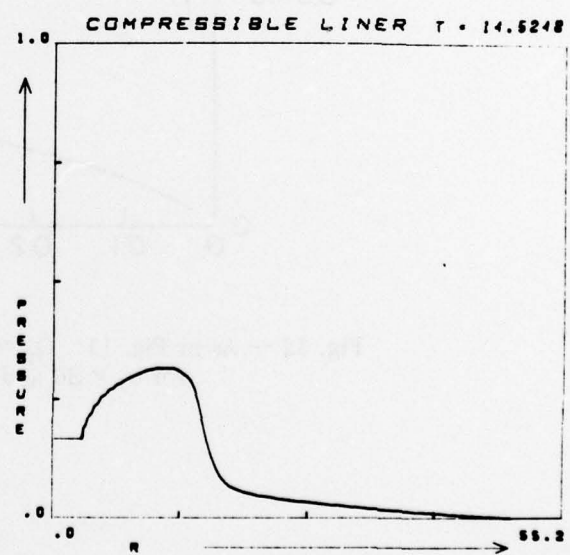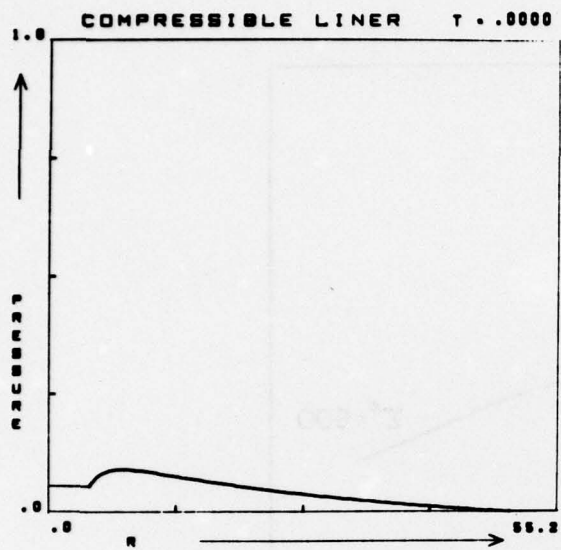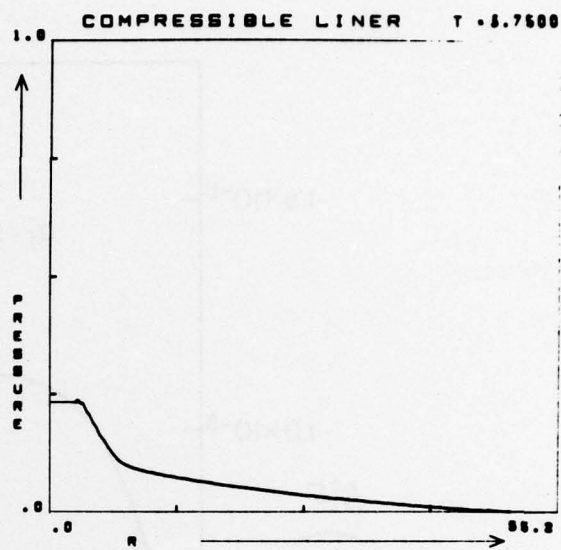
47

COMPRESSIBLE LINER   T = .0000

(a)

COMPRESSIBLE LINER   T = 5.7500

(b)

COMPRESSIBLE LINER   T = 8.5499

(c)

COMPRESSIBLE LINER   T = 14.5248

(d)

48

COMPRESSIBLE LINER   T = .0000

COMPRESSIBLE LINER   T = 5.7500

COMPRESSIBLE LINER   T = 8.5499

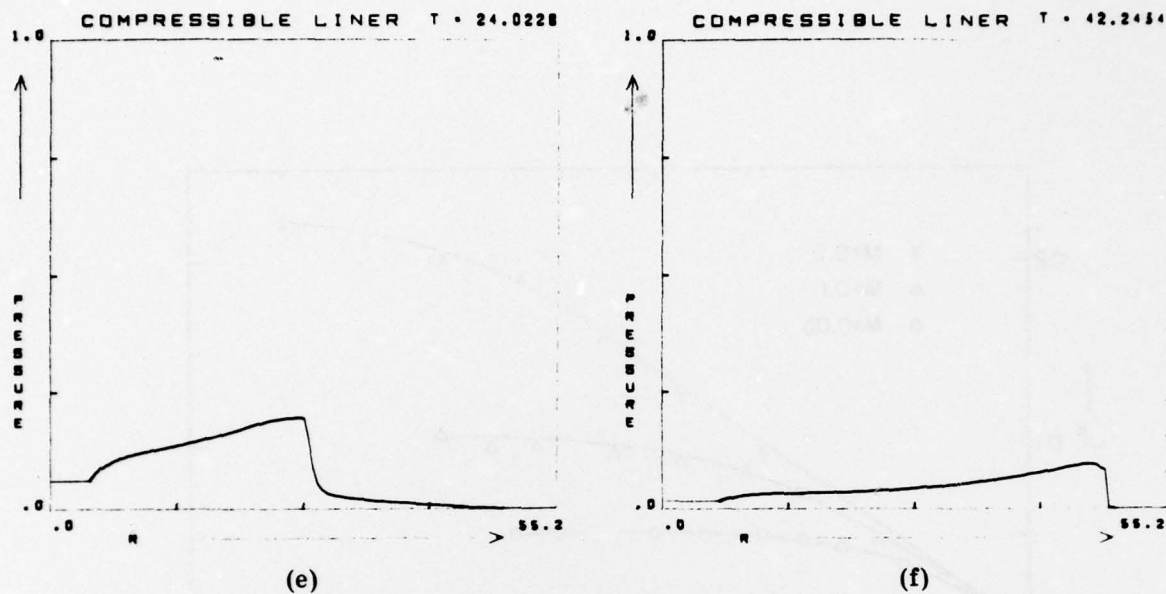COMPRESSIBLE LINER   T = 14.5248

(a)

(b)

(c)

(d)

48
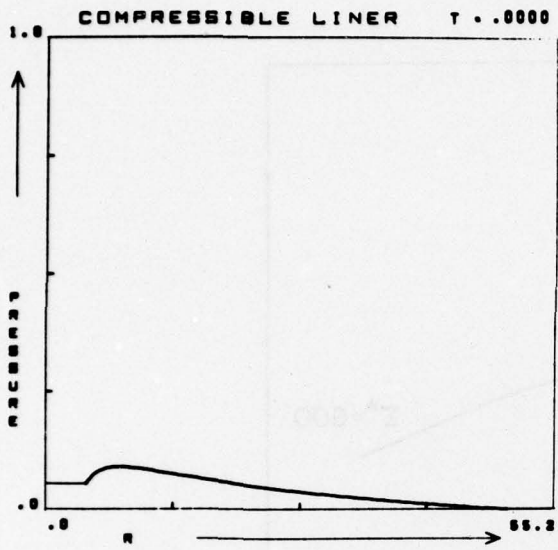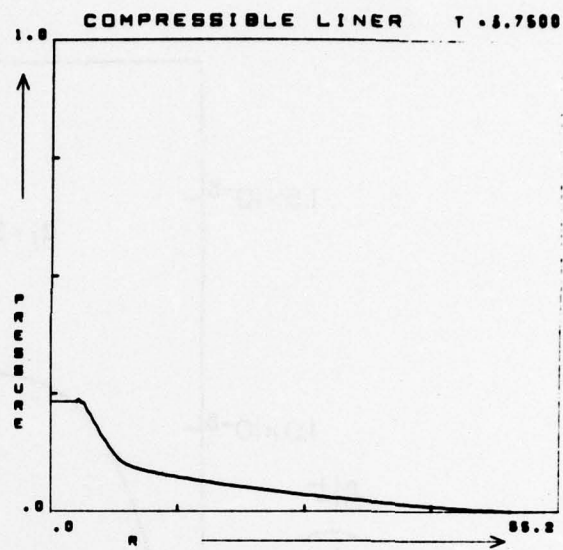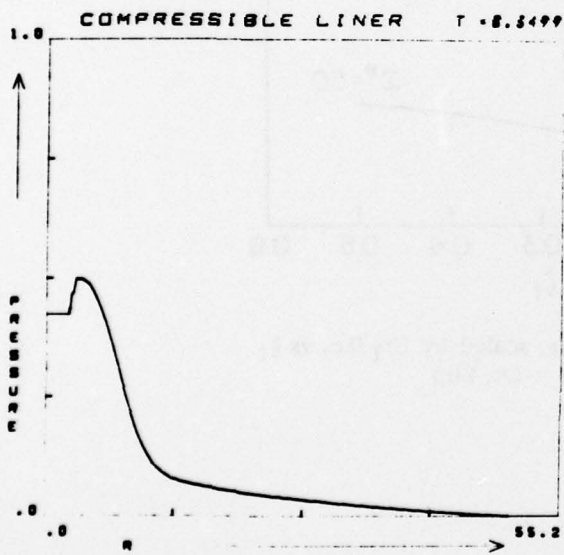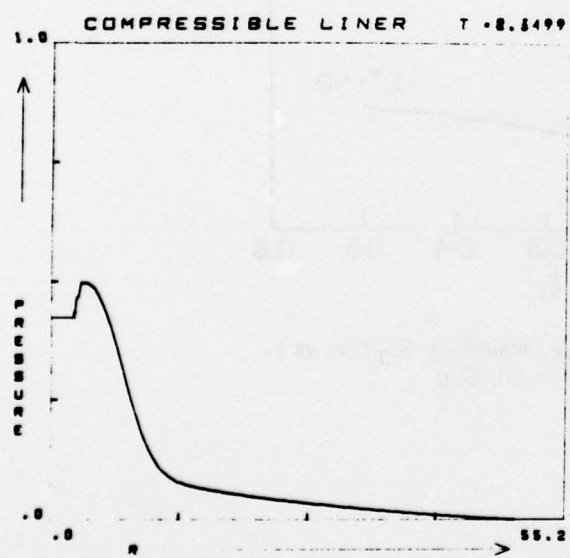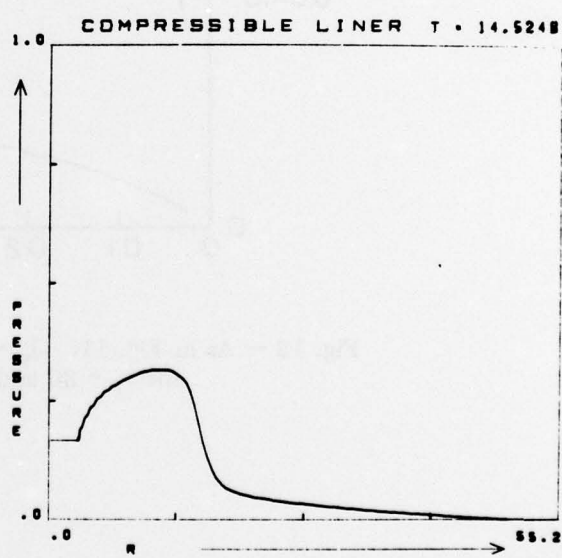
Fig. 13 — Development of water hammer. Pressure profile is shown at initialization (a), shortly before turnaround (b), immediately after turnaround (c), and in various stages as the steep pressure pulse propagates outward (d-f). Time and displacement are scaled by c and r_0.

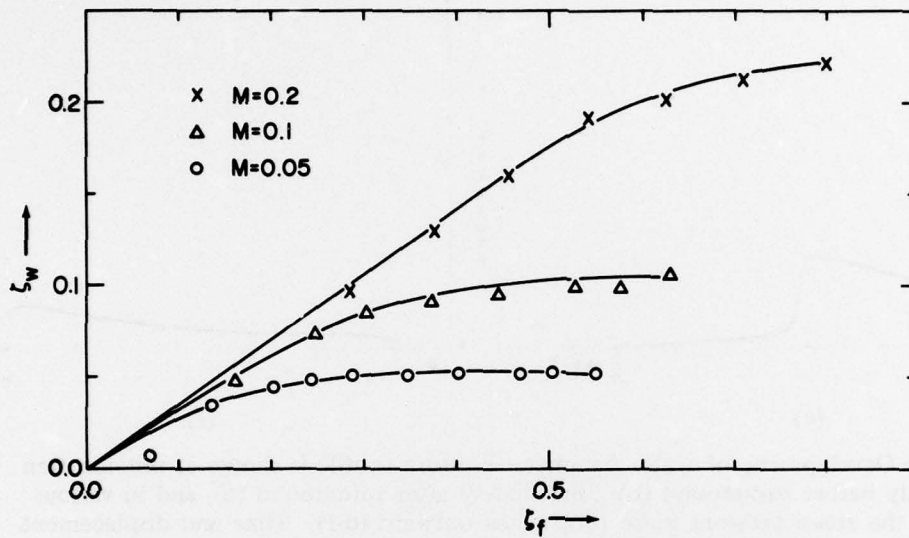Fig. 14 — Dimensionless pressure ζ_w extrapolated to sidewall vs ζ_f
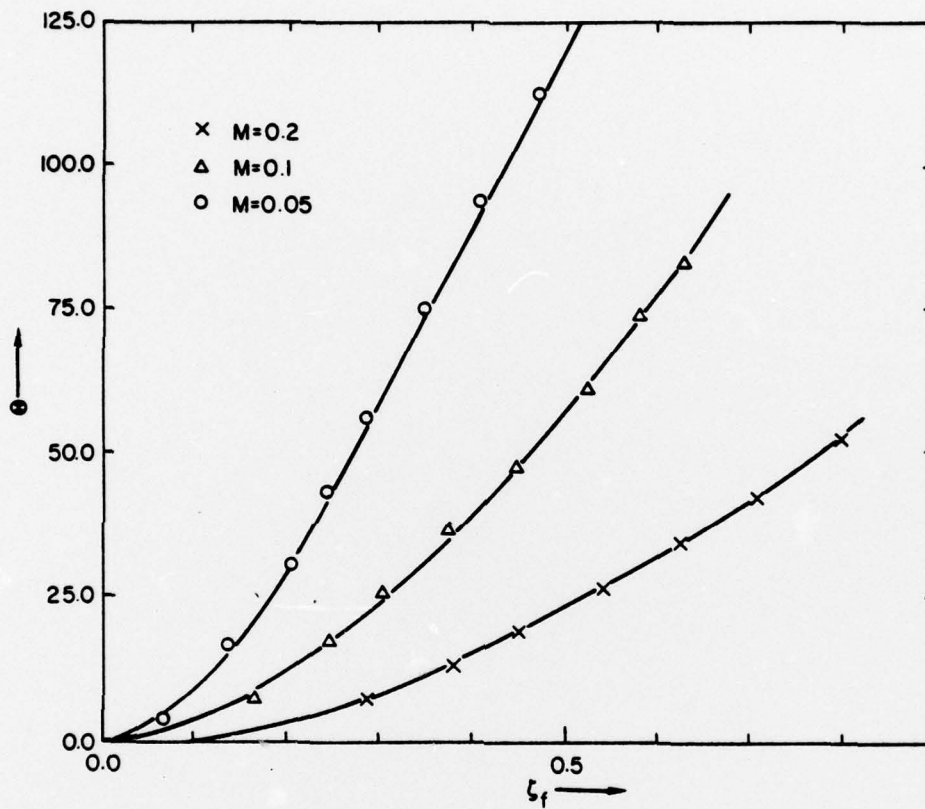for cases A-C (M = 0.2, 0.1, 0.05)

50

Fig. 15 — Dimensionless endwall thrust Θ vs ζ_f for same cases as in Fig. 14